

A Large Deviation Theory-based Analysis of Heat Waves and Cold Spells in a Simplified Model of the General Circulation of the Atmosphere

Vera Melinda Gálfi (1,2), Valerio Lucarini (1,3,4), Jeroen Wouters (3,5)

(1) Meteorological Institute, CEN, University of Hamburg, Hamburg, Germany, (2) IMPRS-ESM, Max Planck Institute for Meteorology, Hamburg, Germany, (3) Department of Mathematics and Statistics, University of Reading, Reading, UK, (4) Center for the Mathematics of Planet Earth, University of Reading, Reading, UK, (5) Niels Bohr Institute, University of Copenhagen, Copenhagen, Denmark

July 13, 2022

Abstract

We study temporally persistent and spatially extended extreme events of temperature anomalies, i.e. heat waves and cold spells, using Large Deviation Theory. To this end, we consider a simplified yet Earth-like general circulation model of the atmosphere and numerically estimate large deviation rate functions of near-surface temperature in the mid-latitudes. We find that, after a re-normalisation based on the integrated autocorrelation, the rate function one obtains at a given latitude by looking, locally in space, at long time averages agrees with what is obtained, instead, by looking, locally in time, at large spatial averages along the latitude, as a result of scale symmetry in the spatial-temporal turbulence and of the fact that advection is primarily zonal. This agreement hints at the universality of large deviations of the temperature field. Furthermore, we discover that, when considering spatio-temporal averages, the obtained rate function is able to describe spatially extended and temporally persistent heat waves or cold spells. Extreme Value Theory is used to benchmark our results.

1 Introduction and Motivation

The typical way to formalise the analysis of extremes for a stochastic variable X revolves around looking at the tail of the probability distribution of X and identifying extremes as very large (or very small) events with long return time. This point - as discussed below - is mathematically very powerful, but in the usual setting is not well suited for studying, in the case of spatio-temporal chaos, anomalously large or small events that are persistent in time and extended in space. *Persistent climatic extreme events* - like heat waves or cold spells - can have a huge impact: they do not affect only human health, but also ecosystems; they can be a danger for our infrastructures and crops, and have a destabilising effect over entire societies; the scale of damage depends critically on the persistent nature and spatial extent of the events. (Easterling et al., 2000; Robinson, 2001; WHO, 2004; IPCC, 2012). Among

the most relevant historical examples we would like to mention the mega-drought that played a major role in the collapse of the Maya empire (Kennett et al., 2012), and the recurrent extreme cold spell episodes referred to as Dzud that led to various waves of migration of the nomadic Mongolian populations (Fang and Liu, 1992; Hvistendahl, 2012).

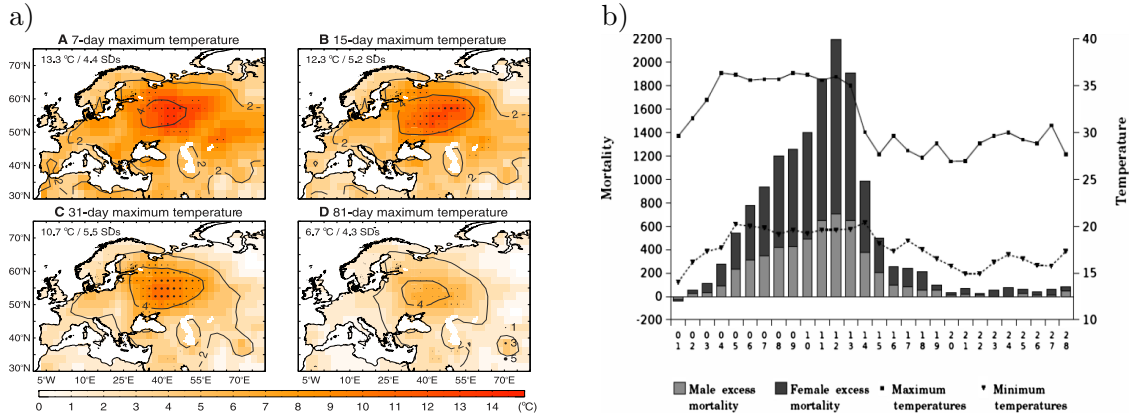


Figure 1: Spatio-temporal features of heat waves and their impacts of health. Panel a): Anomalies of the temperature maxima over four different time scales during the 2010 heat wave. Contour lines indicate the anomalies divided by the climatological standard deviation of temperature in the same location during summer days. The record breaking locations are indicated with dots. The absolute maxima are indicated in the top left corners. Reproduced from Barriopedro et al. (2011). Panel b): Number of excess deaths in France in August (calendar days on the month indicated in the x-axis) during the 2003 heat wave. Note that the number of daily excess deaths increases day by day during the heat wave, and goes rapidly to zero afterwards. Reproduced from Poumadere et al. (2005).

A heat wave or a cold spell is not only lasting for a long time (from several days to several weeks, even months) but has also a considerable spatial extension. For example, the 2003 and 2010 European heat waves had a temporal and spatial extent of the order of weeks to months and 10^6 km^2 respectively (Barriopedro et al., 2011). Anomalous conditions are primarily caused by anomalous synoptic conditions, and, in the case of the mid-latitudes, by atmospheric blocking situations, so we talk about persistence in space and time on *large synoptic scales* (Vautard et al., 2011; Sillmann et al., 2011; Stefanon et al., 2012). In Fig. 1a we portray the intensity and extent of the 2010 heat wave and, in Fig. 1b, we show how the excess fatalities observed in France during the 2003 heat wave increase dramatically as a result of persistent large positive anomalies of temperatures (Poumadere et al., 2005).

It is well known that in the climate system there is a non-trivial relationship between spatial and temporal scales of variability - with large spatial scales associated, in a nontrivial way, to longer time scales. An effective way to represent such relationship is through the so-called Hayashi spectra (Hayashi, 1971; Fraedrich and Boettger, 1978; Speranza, 1983; Dell'Aquila et al., 2005). The existence of such relationship comes from the fact that one can loosely identify different dynamical regimes, each characterised by specialised dynamical balances between the forces acting on the fluid components (Lucarini et al., 2014). Such balances can be rigorously derived via asymptotic analysis applied on the Navier-Stokes equations on a rotating frame of reference (Klein, 2010).

1.1 A Mathematical Framework for Climatic Extremes

1.1.1 Extreme Value Theory

A robust mathematical framework for the study of extreme values is provided by extreme value theory (EVT). Two of the most widely used methods of EVT are the Block Maxima (BM) (Fisher and Tippett, 1928; Gnedenko, 1943) and the Peak Over Threshold (POT) (Pickands, 1975; Balkema and de Haan, 1974) approaches, which differ mostly in the selection procedure of extreme events. Whereas the BM method identifies extremes as maxima M_m of independent identically distributed (i.i.d.) random variables (r.v.) separated into sufficiently large blocks of size m as $m \rightarrow \infty$, the POT approach considers exceedances of a stochastic variable X above a given threshold u as $u \rightarrow x_*$, where x_* represents the upper end point of the distribution of X . Both methods are formulated in form of limit laws, and rely on the convergence in distribution of the selected extreme values to one limiting family of distributions, as one considers more and more extreme levels (i.e. for increasing n or u). Therefore EVT is often interpreted as an analogy to the Central Limit Theorem (CLT). The limiting family of distributions is the Generalized Extreme Value (GEV) distribution in case of the BM method, and the Generalized Pareto distribution (GPD) in case of the POT approach. If the limiting GEV or GPD distributions exist and can be estimated reliably, one can calculate the probability of occurrence of events that are *more extreme* than any observed event. In other words, reliable estimates of return periods for time ranges longer than what is actually observed can be constructed. This indicates that if the limit law applies, predictive power (in a statistical sense) emerges for events with very low probability of occurrence.

As clearly emerges from the discussion above, EVT-based analysis is in principle extremely useful exactly for those stakeholders that need to plan for long time ahead, and has in fact long been applied in areas such as finance (Embrechts et al., 1997), engineering (Castillo, 1988), and hydrology (Katz et al., 2002). Somewhat surprisingly, while examples of application can obviously be found, the methods of EVT are still not the mainstream approach for studying very intense events in climate studies, where it is more popular to use empirical methods based on the analysis of high (or low) percentiles of the probability distribution of the variable of interest. In fact, it is usually assumed that EVT is too data-hungry for being effectively applied in most available climatic time series (IPCC, 2012). Nonetheless, it has been recently shown that EVT can be rigorously and robustly applied also in case of relatively short time series of a few tens of years, see e.g. Zahid et al. (2017).

We have mentioned above the problem of persistence. One can analyse persistent events generally in two ways: first, by treating them as a concatenation of successive extreme events and study the properties of clusters of extremes (Ferro and Segers, 2003; Segers, 2005), or, second, by looking at pdf's of *time-averaged observables*. In this study we follow the second route. Following intuition, if we look at the pdf of finite-size averages of an observable, one expects that the tails of the distribution are mainly populated by averages coming from persistent extremes. A rationale for this is that the averaging window acts like a low-pass filter on the length of the considered persistent events, leading to a connection between extremes of averages and persistent events with a certain length (greater or approximately equal to the chosen averaging window). This will roughly be, in fact, the scenario we will explore below. However, the link between persistence and extremes of finite-size averages is not always true: in case of heavy-tailed r.v., for example, the extremes of averages are

dominated by a single very large extreme event within the averaging window (Mikosch and Nagaev, 1998). We remark that, generally, the methods of EVT can be applied the same way also to study extremes of averaged observables. However, the averaging process reduces the number of available data, so that these methods can become more difficult to apply.

1.1.2 Large Deviation Theory

A mathematical framework describing properties of pdf's of *averaged* observables is provided by Large Deviation Theory (LDT), introduced by Cramer (1938) and further developed by other mathematicians, like Donsker and Varadhan (1975a,b, 1976, 1983), Gärtner (1977), and Ellis (1984). The central result of LDT consists of writing the probability of averaged random variables $A_n = \frac{1}{n} \sum_{i=1}^n X_i$ as function of the variables X_i : for $n \rightarrow \infty$ the probability of averages decays exponentially with n , $p(A_n = a) \approx e^{-nI(a)}$. This is called a large deviation principle (LDP). The speed of decay is described by the so called rate function $I(a) \geq 0$. The probability $p(A_n = a)$ decays everywhere with increasing n , except when $I(a) = 0$. Here $e^{-nI(a)} = 1$. For an i.i.d r.v. one would have that $\mathbb{E}[A_n] = a^*$, where a^* is such that $I(a^*) = 0$. If the rate function exists, one can estimate the probability of averages for every n . Similarly to EVT, if the limit law applies, we gain predictive power, with the difference that in this case it is directed towards averages with increasing n . This means that one does not have to deal anymore with the problem of decreasing amount of data as n increases. LDT is used very extensively in physics, mostly in the context of thermodynamics and statistical mechanics. In the case of an equilibrium system, the global minimum of $I(a)$ represents the system state with maximum entropy, which is at the same time the most probable state, according to the maximum entropy principle. In the case of a non-equilibrium system, under suitable assumptions, rate functions are computed taking into account the time evolution and for each observable the minimum of the rate function defines its expectation value.

While they have recently been applied in the context of geophysical flows (see e.g. Bouchet and Venaille 2012; Bouchet et al. 2014; Herbert 2015), techniques of LDT have been used sporadically until now in climate studies, despite the fact that they can be useful whenever the connection between macroscopic or long term observables and microscopic or instantaneous observables is important, and one is interested in persistent and/or extended fluctuations of a climatic field.

One area of climate modelling where techniques of LDT are just beginning to be applied is the sampling of rare events. Rare event computation techniques based on elements of LDT have been developed with the aim to produce reliable statistics of specific rare events of a given model, as an alternative to long direct numerical simulations (Giardina et al., 2016; Wouters and Bouchet, 2016; Lestang et al., 2018). Ragone et al. (2017) describes how model trajectories can be selected, based on a rare event algorithm, by keeping an ensemble realisation of the system in states that are preferentially close to those leading to heat waves. Therefore, one can exponentially oversample events that have ultra long return periods, and thus construct a richer statistics of heat waves than one would get by standard Monte Carlo techniques. The described method provides also the possibility to investigate dynamical properties of the system state (like global circulation patterns and jet stream position) supporting the occurrence of the studied extremes (heat waves).

1.2 This Paper

In this work we adopt LDT to analyse the properties of temporally and/or spatially persistent surface temperature extremes - heat waves or cold spells - generated through simulation performed with the Portable University Model of the Atmosphere (PUMA) (Lunkeit et al., 1998; Fraedrich et al., 2005b). We investigate temperature averages computed in time and/or in space, the spatial averaging being performed along the zonal direction for reasons of symmetry.

PUMA - details given in Sec. 3 - describes with a good level of precision the dynamics of the three-dimensional atmosphere as an out-of-equilibrium forced-dissipative system. We analyse the properties of the steady state achieved as a result of time-independent forcing after transient dynamics has been discarded. For a wide range of parameter values PUMA features high-dimensional chaotic dynamics (De Cruz et al., 2018). By considering the connection between the averaged values and persistent events on suitably defined scales (as explained above), large deviations of temperature can possibly be related to persistent extreme events of temperature, i.e. heat waves or cold spells.

Following the discussion above, we expect to find a link between spatially extended and temporally persistent events. In order to achieve a large deviation when considering spatial averages in a turbulent system, we need to have occurrence of a spatially extended structure of length say L . In a system possessing a characteristic velocity scale U one expects such a structure to persist for a typical time of the order $\tau = L/U$. Because persistent events are space-time events, we explore the connection between temporal and spatial large deviations, and we also analyse spatio-temporal large deviations. We seek answers to two main questions:

1. How well does LDT describe persistent in space and/or time temperature fluctuations in PUMA?
2. What is the link between temporal, spatial, and spatio-temporal large deviations?

These questions are potentially relevant, because, if we find experimental proofs that the LDP does hold in the case of our numerical simulations, there is a good chance to calculate the probability of occurrence of arbitrarily long in time and/or extended in space (within the limits allowed by the geometry of the Earth, as seen later) heat waves and cold spells.

In the case we find a link between temporal and spatial large deviations, we can deduce the probability of spatial (or spatio-temporal) averages from the one of temporal averages and vice-versa. This can be very useful in case of applications, when for example only temporal or only spatial series are available. In order to test the quality of the predictions of the return time based on LDT, we compare the results with what can be obtained using EVT (we use the POT method).

The structure of the paper is as follows. In Section 2, we provide the theoretical formulation of LDT and some elements of EVT. In Section 3 we give a description of the model PUMA and give details of the numerical simulations performed for the scopes of this paper. We then present our results in Section 4. Here, we first focus on the link between temporal and spatial large deviations, and then we additionally consider the case of spatio-temporal large deviations. We test the correctness and applicability of our results by computing return periods of extremes of temperature averages and comparing them with the empirical data

and return periods obtained based on the POT method. Section 5 concludes the paper with a summary and discussion of our results.

2 Some Elements of Large Deviation Theory and of Extreme Value Theory

2.1 Constructing the Rate Functions Describing the Large Deviations

The large deviation theoretical framework can be formulated on three different levels, corresponding to the complexity of the statistical description of the dynamical system. These are, as described by Oono (1989), based on: sample means of observables (level-1), probability distributions on the state space of observables (level-2), and probability distributions on the path or history space, i.e. the entire set of possible orbits or histories of the system (level-3). The below description follows the level-1 approach, according to the scientific purpose of this paper, and is mostly based on the works of Touchette (2009) and Oono (1989). We do not pursue at all a rigorous mathematical formulation here; our aim is rather to recapitulate the main concepts and results, and to introduce our notation. We also give some physical interpretations of the main mathematical concepts.

We say that the r.v. $A_n = \frac{1}{n} \sum_{i=1}^n X_i$, where X_i are identically distributed r.v.s, satisfies a large deviation principle (LDP) if the limit

$$\lim_{n \rightarrow \infty} -\frac{1}{n} \ln p(A_n = a) = I(a) \quad (1)$$

exists. $I(a) \geq 0$ is the so-called rate function, representing the rate of the exponential decay. The probability density $p(A_n = a)$ decays exponentially with n for every value of a except the ones for which $I(a) = 0$, where $\lim_{n \rightarrow \infty} p(A_n = a^*) = 1$, and $a^* = \mathbb{E}[A_n]$. Whenever this limit holds and $I(a)$ has a unique global minimum, A_n converges in probability to its mean a^* and obeys the Law of Large Numbers. If then additionally $I(a)$ is quadratic (i.e. twice differentiable) around a^* , the Central Limit Theorem (CLT) holds, meaning that small fluctuations around the mean are normally distributed. The expression “small fluctuations” is very important here, because large fluctuations around the mean are not necessarily normally distributed. Since the rate function describes both small and large deviations, LDT can be considered as a generalisation of CLT.

Now let's consider, instead of r.v.s, observables produced by a deterministic dynamical system. If the system is Axiom A, all of its observables obey a LDP (Eckmann and Ruelle, 1985). If we consider a system whose dynamics is characterised by high-dimensional chaotic dynamics, by invoking the chaotic hypothesis introduced by Gallavotti and Cohen (1995), one can expect to find large deviation laws, even in systems which are not Axiom A.

The dynamical nature of out-of-equilibrium steady state systems requires, however, a slight modification of our theoretical approach, which mainly implies that time has to be considered in the formulation of the LDP, replacing the parameter n . Due to temporal correlations in these systems the computation of the rate function requires level-2 or level-3 theory. This has been done for Markov chains and r.v. with a specific form of dependence, and involves

mostly the computation of transition matrices or joint pdf's (den Hollander, 2000; Touchette, 2009). In case of non-Markovian processes and high dimensional systems the computation of analytical rate functions is a hopeless endeavour. Thus, in this work, we adopt another (very simple) strategy in dealing with temporal correlations. In case of weakly correlated observables (i.e. X_j and X_l have an exponentially decreasing correlation if $|j - l|$ is large enough), one can take advantage of the fact that for large enough n the averages A_n become almost uncorrelated. This represents the basis for the block averaging method (Rohwer et al., 2015). We transform the variables X_i into variables $Y_i = \frac{1}{b} \sum_{i=1}^b X_i$, where b represents the size of the averaging block, i.e $b = n/k$ with the number of blocks k . In case Y_i are almost independent and identically distributed (ergodic Markov chain), a large deviation principle can be obtained for:

$$A_n = \frac{1}{k} \sum_{i=1}^k Y_i = \frac{1}{n} \sum_{i=1}^n X_i. \quad (2)$$

Intuitively, one can argue that b has to be at least so large that X_1 and X_b are almost uncorrelated, i.e. $b \geq \rho$ where ρ is a metric of persistence expressed in terms of number of successive correlated data. One usually quantifies persistence in terms of the auto-correlation function. Considering our scientific goal, which is the study of probabilities of averages, it makes sense to choose the integrated auto-correlation as a general measure of patterns in time and space, since this quantity plays a central role in the formulation of the CLT for Markov chains, as described below.

According to a formulation of CLT in case of dependent variables based on Billingsley (1995), suppose that X_1, X_2, \dots is a stationary Markov chain with $\mathbb{E}[X_n] = 0$ and satisfies appropriate mixing conditions, then the variance of the sample mean A_n is

$$n\mathbb{E}[A_n^2] \rightarrow \mathbb{E}[X_1^2] \left(1 + 2 \sum_{k=1}^{\infty} c(k)\right) \quad (3)$$

where $c(k) = \frac{C(k)}{C(0)}$ is the auto-correlation, and $C(k)$ denotes the auto-covariance at lag k , $C(k) = \mathbb{E}[X_i X_{i+k}]$. Eq. (3) shows that the rescaled variance of the sample mean of the Markov chain converges to the variance of X_1 times the integrated auto-correlation.

2.2 Extreme Value Theory: Peaks over Threshold Approach

As explained above, based on LDT one can estimate small and large deviations. In this work, however, we are especially interested in large deviations, which can be also interpreted as extremes of averaged quantities. Therefore, it is straightforward to analyse the extremes of averages based on EVT. Note that, although the application of EVT to averaged observables can be difficult in applications due to the decrease of the data amount by averaging, our numerical simulations are long enough to allow for a reliable implementation of EVT also in the case of averages. With the aim of drawing a broader picture, we additionally apply the POT approach of EVT, which is briefly described in the following.

Let us consider $Z_m = \max\{X_1, \dots, X_m\}$, where X_1, \dots, X_m is a sequence of i.i.d. r.v. with common distribution function $F(x)$. The Fisher-Tipett-Gnedenko theorem (Fisher and Tip-

pett, 1928; Gnedenko, 1943) states that the distribution of properly normalised block maxima Z_m converges under certain conditions, for $m \rightarrow \infty$, to the so-called Generalized Extreme Value (GEV) distribution $G(z; \mu, \sigma, \xi)$, with three parameters: location parameter μ , scale parameter σ , and shape parameter ξ .

Pickands (1975) reformulated the Fisher-Tipett-Gnedenko theorem based on the conditional probability of values exceeding a high threshold u and reaching the upper right point of the distributions of X , given that $X > u$. Under the same conditions, for which the distribution of Z_m converges to the GEV distribution, the exceedances $y = X - u$ are asymptotically distributed according to the Generalized Pareto distribution (GPD) family (Coles, 2001)

$$H(y; \tilde{\sigma}, \tilde{\xi}) = \begin{cases} 1 - \left(1 + \frac{\tilde{\xi}y}{\tilde{\sigma}}\right)^{-1/\tilde{\xi}} & \text{for } \tilde{\xi} \neq 0, \\ 1 - \exp\left(-\frac{y}{\tilde{\sigma}}\right) & \text{for } \tilde{\xi} = 0, \end{cases} \quad (4)$$

where $1 + \tilde{\xi}y/\tilde{\sigma} > 0$ for $\tilde{\xi} \neq 0$, $y > 0$, and $\tilde{\sigma} > 0$. $H(y)$ has two parameters: the scale parameter $\tilde{\sigma}$ and the shape parameter $\tilde{\xi}$. The shape parameter $\tilde{\xi}$ describes the decay of probabilities in the tail of the distribution, and determines to which one of the three possible types of GPD distributions $H(y)$ belongs. If $\tilde{\xi} = 0$, the tail decay is exponential; if $\tilde{\xi} > 0$, the tail decay is polynomial; and if $\tilde{\xi} < 0$ the distribution is bounded (Pickands, 1975; Balkema and de Haan, 1974), i.e. the extremes are limited from above. In case of convergence to the GEV and GPD distributions, $\tilde{\xi} = \xi$ and $\tilde{\sigma} = \sigma + \xi(u - \mu)$ (Coles, 2001).

Classical EVT has been extended and adapted to analyse extremes of observables of chaotic dynamical systems. A detailed overview of this research field is provided by Lucarini et al. (2016). If one considers an Axiom A system, one obtains that EVT of different classes of observables can be used to infer the properties of the stable and unstable manifold, including the possibility of estimating the Kaplan-Yorke dimension (Eckmann and Ruelle, 1985). Just as discussed above, adopting the chaotic hypothesis (Gallavotti and Cohen, 1995), such findings can be expected to apply for more general systems possessing high-dimensional chaos; see a detailed analysis in (Bódai, 2017) and an accurate investigation in the case of a high-dimensional system in (with $O(10^3)$ degrees of freedom) in Galfi et al. (2017). EVT combined with the analysis of recurrences has proved very useful for providing a new framework for identifying the so-called weather patterns in actual climate data and in the outputs of climate models, and for interpreting their specific dynamical properties (Faranda et al., 2017; Messori et al., 2017).

2.3 Return Periods and Return Levels

We compare the two methods of analysing rare events on a practical level, i.e. based on return periods and return levels. In case of LDT, we estimate the return periods of events exceeding the value a as $\frac{1}{1 - \tilde{P}(A_n \leq a)}$, where $\tilde{P}(A_n \leq a)$ represents the cumulative distribution function. In case of the POT approach, the expected return levels or extreme quantiles are obtained from the values of the GPD parameters, which can be inferred using usual proven estimation methods, like maximum likelihood estimation (Coles, 2001) or L-moments (Hosking, 1990). The level y_m that is exceeded on average once every m -observations is called the m -observation return level and is the solution of $P(Y > y) = \frac{1}{m}$. One obtains $P(Y > y)$

from $H(y) - 1 = P(Y > y | Y > u) = \frac{P(Y > y)}{P(Y > u)}$, and consequently (Coles, 2001):

$$y_m = \begin{cases} u - \frac{\tilde{\sigma}}{\tilde{\xi}} \left[1 - \left(\frac{1}{mP(Y > u)} \right)^{-\tilde{\xi}} \right] & \text{for } \tilde{\xi} \neq 0, \\ u - \tilde{\sigma} \log\left(\frac{1}{mP(Y > u)}\right) & \text{for } \tilde{\xi} = 0. \end{cases} \quad (5)$$

As an effect of serial correlations, the threshold exceedances can be organised in clusters. If an extreme value law does exist at all in this case, it is necessary to introduce the so-called extremal index - the inverse of the limiting mean cluster size - which has to be considered in the estimation of the GPD parameters, with the exception of the shape parameter (Coles, 2001). A widely adopted method to deal with correlated threshold excesses is to apply declustering, which basically aims to identify the maximum excess within each cluster and then to fit the GPD distribution to the cluster maxima (Leadbetter et al., 1989; Ferro and Segers, 2003). Here, we consider extremes of nearly uncorrelated series of averages, thus the POT approach can be applied in a straightforward way, similarly to the case of i.i.d. r.v..

3 Model Description and Setup

We perform simulation with the Portable University Model of the Atmosphere (PUMA), which is a simplified spectral general circulation model (GCM) developed at the University of Hamburg. PUMA has been used for the investigation of several atmospheric phenomena, like storm track dynamics or low frequency variability (Lunkeit et al., 1998; Fraedrich et al., 2005b), and has been even adapted to extra-terrestrial atmospheres (Grieger et al., 2004). A recent study investigates the properties of the Lyapunov spectrum in PUMA, including large deviations of finite time Lyapunov Exponents (De Cruz et al., 2018). PUMA is the dry core of the Planet Simulator (PlaSim), which is a climate model of intermediate complexity (Fraedrich et al., 2005a; Lucarini et al., 2010).

In the following, we summarise the model equations and the applied parametrisations. For a more detailed description of the model, please consult Fraedrich et al. (2009). As commonly done in atmospheric modelling, the physics of the model is fundamentally described by the primitive equations for the atmosphere, which amount to a modification of the Navier-Stokes equation in a rotating frame of reference where the vertical acceleration of the fluid is constrained to be small compared to gravity (Klein, 2010). These equations provide a good representation of the dynamics of the atmosphere for horizontal spatial scales large than few tens of kms (Holton, 2004). Compared to a full atmospheric GCM, moist processes are omitted, and simple parametrisations are used to account for the effect of friction (Rayleigh friction), diabatic heating (Newtonian cooling), and diffusion. The Newtonian cooling and Rayleigh friction terms are such as that proposed by Held and Suarez (1994) for the comparison of dynamical cores of GCMs. The model equations allow for the conservation of momentum, mass, and energy. The prognostic equations for absolute vorticity ($\zeta + f$), divergence D , temperature T , and surface pressure p_s can be written by using spherical coordinates and the vertical σ -system as follows:

$$\frac{\partial(\zeta + f)}{\partial t} = \frac{1}{1 - \mu^2} \frac{\partial F_v}{\partial \lambda} - \frac{\partial F_u}{\partial \mu} - \frac{\zeta}{\tau_F} - K \nabla^8 \zeta \quad (6)$$

$$\frac{\partial D}{\partial t} = \frac{1}{1 - \mu^2} \frac{\partial F_u}{\partial \lambda} + \frac{\partial F_v}{\partial \mu} - \nabla^2 \left(\frac{U^2 + V^2}{2(1 - \mu^2)} + \Phi + T_0 \ln p_s \right) - \frac{D}{\tau_F} - K \nabla^8 D \quad (7)$$

$$\frac{\partial T'}{\partial t} = -\frac{1}{1 - \mu^2} \frac{\partial(UT')}{\partial \lambda} - \frac{\partial(VT')}{\partial \mu} + DT' - \dot{\sigma} \frac{\partial T}{\partial \sigma} + \kappa \frac{T}{p} \omega + \frac{T_R - T}{\tau_R} - K \nabla^8 T \quad (8)$$

$$\frac{\partial \ln p_s}{\partial t} = - \int_0^1 D + \vec{V} \cdot \nabla \ln p_s d\sigma \quad (9)$$

with

$$F_u = V(\zeta + f) - \dot{\sigma} \frac{\partial U}{\partial \sigma} - T' \frac{\partial \ln p_s}{\partial \lambda}$$

$$F_v = -U(\zeta + f) - \dot{\sigma} \frac{\partial V}{\partial \sigma} - T'(1 - \mu^2) \frac{\partial \ln p_s}{\partial \mu}.$$

The variables and parameters used in Eq. (6) – (9) are listed in Table 1.

Table 1: list of variables and parameters in puma, eq. (6) – (9).

symbol	value	description
$\zeta = \frac{\partial v}{\partial x} - \frac{\partial u}{\partial y}$		relative vorticity
f		Coriolis parameter
$D = \frac{\partial u}{\partial x} + \frac{\partial v}{\partial y}$		horizontal divergence
T		temperature
T_0	250 K	reference temperature
$T' = T - T_0$		temperature deviation from T_0
p		pressure
p_s		surface pressure
$\sigma = p/p_s$		vertical coordinate
$U = u \cos \phi$		zonal velocity in spherical coordinates
$V = v \cos \phi$		meridional velocity in spherical coordinates
\vec{V}		horizontal velocity with components U and V
t		time
ϕ		latitude
μ		$\sin \phi$
λ		longitude
ϕ		geopotential
$\omega = dp/dt$		vertical velocity in p -system
$\dot{\sigma} = d\sigma/dt$		vertical velocity in σ -system
τ_F		time scale for Rayleigh friction
K		hyperdiffusion coefficient
τ_R		time scale for Newtonian cooling
T_R		restoration temperature
κ	0.286	adiabatic coefficient

The horizontal representation of the prognostic model variables is given by a series of spherical harmonics, which are integrated in time by a semi-implicit time differencing scheme (Hoskins and Simons, 1975). The linear contributions in the prognostic equations are computed in spectral space, the non-linear contributions in grid point space. The horizontal resolution is defined by triangular truncation. The vertical discretization is based on finite differences on equally spaced σ -levels. The vertical velocity is set to 0 at the upper ($\sigma = 0$) and lower ($\sigma = 1$) boundaries.

A Rayleigh damping of horizontal velocities with time scale τ_F accounts for the effect of boundary layer friction in the lowest levels. $\tau_F = 0.6$ days at $\sigma = 0.95$ (the vertical level nearest to surface), and $\tau_F = 1.65$ days at $\sigma = 0.85$. For higher levels no friction is considered, i.e. $\tau_F = \infty$. The effect of non resolved processes on the energy and enstrophy cascade is represented by hyperdiffusion ($\sim \nabla^{2h}$). The hyperdiffusion coefficient K is such that provides a maximal damping of the shortest waves, and has no effect on the mean state (wave number 0). The integer exponent $h = 4$ leads to an additional damping of short waves. The diffusion time scale for the shortest wave is 1/4 days. The diabatic heating (cooling) is parameterized by a Newtonian cooling term. This forces the relaxation of the model temperature to a so-called radiative-convective *equilibrium* state specified by the restoration temperature T_R , which depends only on vertical level and latitude.

$$T_R(\phi, \sigma) = T_R(\sigma) + f(\sigma)T_R(\phi) \quad (10)$$

$T_R(\phi)$ describes the meridional form of the restoration temperature, whereas $f(\sigma)$ accounts for the vertical changes in this meridional profile:

$$T_R(\phi) = (\Delta T_R)_{NS} \frac{\sin \phi}{2} - (\Delta T_R)_{EP} (\sin^2 \phi - \frac{1}{3}), \quad (11)$$

where $(\Delta T_R)_{NS}$ is the temperature difference between the North and South poles, and $(\Delta T_R)_{EP}$ represents the equator-to-pole temperature difference. The meridional temperature gradient decreases with height in the troposphere, $f(\sigma) = \sin(0.5 \pi(\sigma - \sigma_{tp})/(1 - \sigma_{tp}))$ for $\sigma \geq \sigma_{tp}$, and vanishes at the tropopause, $f(\sigma) = 0$ for $\sigma < \sigma_{tp}$, where σ_{tp} is the height of the tropopause. $T_R(\sigma)$ describes the vertical profile of the restoration temperature:

$$T_R(\sigma) = (T_R)_s - Lz_{tp} + \sqrt{\left[\frac{L}{2}(z_{tp} - z(\sigma))\right]^2 + S^2} + \frac{L}{2}(z_{tp} - z(\sigma)), \quad (12)$$

with: restoration temperature at the surface, $(T_R)_s = 288$ K; moist adiabatic lapse rate, $L = 6.5$ K/km; global constant height of the tropopause, $z_{tp} = 12$ km; geometric height z . S allows for a smoothing of the temperature profile at the tropopause. In case of 10 vertical levels l , the time scale of the Newtonian cooling τ_R is 2.5 days in the lowest level at $l = 10$, and 7.5 days at $l = 9$. τ_R continues to increase monotonically with height until the upper 3 levels, where it is set to 30 days.

We run the model in a simple symmetric setting (usually referred to as aqua-planet), i.e. without orography. We remove the annual and diurnal cycle, and use a symmetric forcing with respect to the Equator, $(\Delta T_R)_{NS} = 0$. We set the Equator-to-Pole temperature difference $(\Delta T)_{EP}$ to 90 K, thus creating a baroclinically more unstable atmospheric state than in the standard setting with $(\Delta T)_{EP} = 70$ K. We run the model with constant forcing in

time using a time step of 30 minutes. The horizontal resolution is T42 (triangular spectral truncation with 42 zonal waves), and the vertical resolution consists of 10 levels. The length of the simulations is 10^4 years, not counting the first 5 years, which are discarded to reach steady state. We consider for our analysis the air temperature in the lowest vertical level at 960 hPa, with daily output. The spectral temperature variable is transformed during the post-processing into grid point space consisting of a 65×128 equidistant latitude-longitude grid.

Using the same model settings as above, but with a lower Equator-to-Pole temperature difference, De Cruz et al. (2018) estimate a Kaplan-York dimension D_{KY} of 187 and a number of positive Lyapunov exponents of 68 for $(\Delta T)_{EP} = 60$ K. In this study, $(\Delta T)_{EP} = 90$ K, thus the model atmosphere is baroclinically substantially more unstable than in the mentioned study. Thus, to provide a rough estimation, $D_{KY} > 200$ and the number of positive Lyapunov exponents > 80 in our system. Consequently, we expect for this set-up a very high dimensional chaos, which fulfils the chaotic hypothesis, as shown also by the fast decay of auto-correlations in Fig. 2c,d below. As a result, we expect that the outputs of our model can be analysed using EVT and LDT, as discussed above. Nonetheless, it is *a priori* unclear whether the asymptotic result can be clearly detected at finite size given the length of our numerical integrations. Note that in De Cruz et al. (2018) it was shown that the finite time Lyapunov exponents obey a large deviation law¹.

4 Results

Before discussing our main results related to the large deviations of temperature, it is useful to have a general picture about the properties of the simulated temperature field at 960 hPa (i.e. close to the surface). For the analysis of temporal, zonal, and spatio-temporal large deviations, we select three latitudes: 60° , 46° , and 30° (dashed horizontal lines in Fig. 2a). We focus on the mid-latitudes because it is the region of the atmosphere with the strongest turbulence, so that we expect that the corresponding observables should behave in coherence with the chaotic hypothesis; see discussion in Galfi et al. (2017). The two hemispheres are symmetric, thus it is not important which one we consider. In the following, we provide first a qualitative comparison of temporal and spatial characteristics of the temperature field, and then we quantify the persistence in time and space based on the integrated auto-correlation.

Figure 2a illustrates the temperature field $T(x, y, t^*)$ as function of longitude x and latitude y at one selected time point t^* , whereas Fig. 2b represents the temperature field $T(x^*, y, t)$ as function of latitude y and of time t at one selected longitude x^* . Qualitatively similar figures would be obtained for different values of t^* and of x^* , respectively. Note that, to facilitate the comparison between space and time, the x -axis in Fig. 2b is backward in time according to the prevailing eastward zonal wind at mid-latitudes. Additionally, the range of the x -axis

¹This is not always fulfilled in models which incorporate multiscale phenomena, as in the case of coupling atmospheric and oceanic dynamics. In the same study, the authors could not detect large deviation laws in case of a quasi-geostrophic coupled ocean-atmosphere model. Vannitsem and Lucarini (2016) analysed the large deviations of finite time Lyapunov exponents as well in a low-order version of the above mentioned coupled model, and found a LDP only in case of nonzero Lyapunov exponents, whereas the convergence was considerably slower or even absent in case of near-zero Lyapunov exponents.

in Fig. 2b is the same as in Fig. 2b once we rescale the time axis according to the scale velocity U_T introduced below (computed for 46°), which weights the decay of correlation in space at fixed time and in time at fixed location. Comparing these two figures we realise that by cutting across time or across longitudes we obtain very similar wavy patterns, which is non-surprising since the forcing is invariant in time and along a latitudinal band.

While this result would be trivial when observing a periodic or quasi-periodic signal, we need to consider here that the dynamics of the atmosphere features a nontrivial mixture of wave, turbulence, and particles (Ghil and Roberston, 2002), so that we need to look at this space-time similarity from a statistical point of view. According to this, we have that, at a given latitude y^* , the temporal series $T(x^*, y^*, t)$ and the zonal series $T(x, y^*, t^*)$ are sampled from two identically distributed random processes, given the condition of steady state and the discrete symmetry with respect to translation along latitudes.

The main difference is related to distinct temporal and spatial characteristic scales, i.e. to temporal or spatial correlations. At mid-latitudes, cyclones have a typical temporal scale of ≈ 1 day and a characteristic spatial scale of about 1000 km (Holton, 2004). Obviously, these scales are relevant when we try obtain a LDP, thus it is very important to find an adequate metric to describe them. We quantify the typical temporal and zonal scales based on the integrated auto-correlation, as explained in Sec. 2.

We calculate the auto-correlations of the temporal and zonal series at a selected latitude y^* , based on which we obtain later the integrated temporal and zonal auto-correlations. For this, we use 1000 years of our simulation out of a total of 10000 years, as this proves more than enough to reach robust estimates. As explained in Sec. 2, the auto-correlation is defined as the ratio between the auto-covariance $C(l)$ at lag l and the variance σ^2 : $c(l) = C(l)/C(0) = C(l)/\sigma^2$. To obtain better auto-correlation estimates, we calculate the spatio-temporal mean and variance at each y^* , and use these estimates for the computation of both temporal and zonal auto-correlations:

$$\mu = \frac{1}{N_t N_x} \sum_{j=1}^{N_t} \sum_{i=1}^{N_x} T(i, y^*, j)$$

and

$$\sigma^2 = \frac{1}{N_t N_x - 1} \sum_{j=1}^{N_t} \sum_{i=1}^{N_x} (T(i, y^*, j) - \mu)^2,$$

where $N_t = 3.6 \times 10^5$ is the number of considered points in time (daily data), and $N_x = 128$ is the number of grid points in the zonal direction. This is reasonable considering the symmetries in our system in time and along latitudinal circles. The subscripts t and x refer to time and to the zonal dimension, also in what follows.

In case of the temporal series $T(x^*, y^*, t)$, we calculate the auto-covariance at one selected longitude x^* . This estimate is independent of x^* , thus it is unimportant which longitude we choose. We have:

$$c_t(l_t) = \frac{1}{\sigma^2} \frac{1}{N_t} \sum_{i=1}^{N_t-l_t} (T(x^*, y^*, i) - \mu) (T(x^*, y^*, i + l_t) - \mu) \quad (13)$$

The length of the zonal series $T(x, y^*, t^*)$, however, is too short to obtain reliable auto-

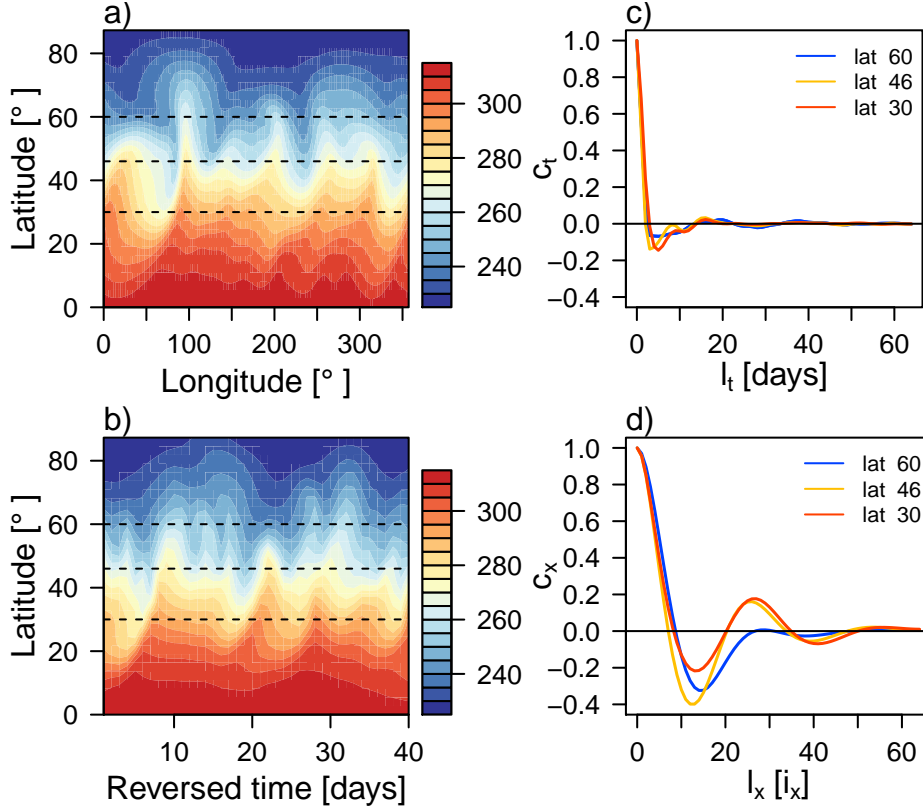


Figure 2: General properties of the temperature field at 960 hPa. a) Temperature values $T(x, y, t^*)$ as function of longitude x and latitude y at one selected time point t^* . b) Temperature values $T(x^*, y, t)$ as function of latitude y and of time t at one selected longitude x^* (the x -axis is backward in time). The dashed lines in a) and b) mark the selected latitudes. c) Temporal and d) zonal auto-correlation functions according to (13) and (14) for the selected latitudes (different colours according to the legend).

correlation estimates. The number of grid points along the zonal dimension is only 128. Together with such a restriction related to the *size* of the Earth, there is another one related to the *shape* of the Earth. In fact, we have to reduce the maximum lag to $N_x/2 = 64$ because at larger lags the correlations start to increase again due to the periodicity along a latitudinal circle. To increase the robustness of our estimate, we first calculate the lagged zonal auto-correlation coefficients at each time point and then we take the average over time:

$$c_x(l_x) = \frac{1}{\sigma^2} \frac{1}{N_x N_t} \sum_{j=1}^{N_t} \sum_{i=1}^{N_x - l_x} (T(y^*, i, j) - \mu) (T(y^*, i + l_x, j) - \mu). \quad (14)$$

Figure 2c shows the temporal auto-correlation coefficient as function of the temporal lag in units of days, whereas Fig. 2d illustrates the zonal auto-correlation coefficient as function of the spatial lag expressed as longitude indexes $i_x = 0, 1, 2, \dots$. Both temporal and spatial auto-correlations decay to zero, meaning that two temperature values, which are far away from each other in time or in space are almost independent. We finally estimate the integrated temporal and zonal auto-correlations by taking the sum of the auto-correlations coefficients

until the maximum lag $l_t = l_x = 64$. Note that we use the same temporal and zonal maximum lags for consistency reasons. The temporal integrated auto-correlation can be obtained also for larger maximum lags, but this changes only negligibly the estimate value because the decay to 0 is relatively fast. We define:

$$\tau_t = 1 + 2 \sum_{l_t=1}^{64} c_t(l_t) \quad (15a)$$

$$\tau_x = 1 + 2 \sum_{l_x=1}^{64} c_x(l_x) \quad (15b)$$

τ_t is 1.32 at 60°, 1.05 at 46°, and 1.61 at 30°, whereas τ_x is 3.26 at 60°, 3.54 at 46°, and 7.68 at 30°. We define τ_t and τ_x in a non-dimensional form (i.e. as number of time units or zonal data points) to facilitate the comparison of temporal and spatial persistence based on the resolution of our data, and because in this form we can use them directly for scaling the rate function, as we show below.

In order to express the temporal and zonal persistence in physical units, one just needs to multiply τ_t by the time step $\delta_t = 1$ day, and τ_x by the zonal grid spacing δ_x , which is latitude dependent. Thus, the temporal persistence expressed in units of days is equivalent to τ_t , and the zonal persistence in units of km amounts to 391 at 60°, 732 at 46°, and 1292 at 30°. We define the scale velocity $U_\tau := \frac{\tau_x \delta_x}{\tau_t \delta_t}$. From a statistical point of view, U_τ represents the ratio between spatial and temporal persistence. From a geometrical/dynamical point of view, U_τ represents the ratio between spatial and temporal typical scales. Thus, U_τ is a measure for the anisotropy between space and time. At 60° $U_\tau = 4.25 \text{ ms}^{-1}$ and at 46° $U_\tau = 8.47 \text{ ms}^{-1}$. U_τ is not necessarily the same as the temporally averaged zonal mean wind \overline{U} (at the same vertical level of 960 hPa), although, clearly, a dynamical relationship exists, because the turbulent structures are advanced, to a first approximation, by the mean flow. In fact, we find that \overline{U} is 3.6 ms^{-1} at 60°, and 6 ms^{-1} at 46°, which bear a good agreement with the scale velocities at the same latitudes.

The agreement is lost when looking at 30°, which is at the boundary of the mid-latitude baroclinic zone where the qualitative description given above applies. As we approach the equator, the atmospheric dynamics has a much lower degree of chaoticity with respect to the mid-latitudes, unless we look at the convective scales, which are not resolved at all in this model, and spatial persistence is very enhanced (see also Fig. 2a,b). In this case we find $U_\tau = 14.95 \text{ ms}^{-1}$, while \overline{U} is -3.4 ms^{-1} , which indicates prevailing easterly flow, a clear signature of tropical dynamics.

Before continuing with the description of the temporal and spatial large deviations, we briefly discuss the connection between high values of coarse grained temperatures and long individual events where the temperature readings are persistently above the long-term average, discussed already in Sec. 1. Fig. 3a,b,c show three short temporal series at latitude 46° together with the corresponding series of the coarse grained quantities where averages are computed using block lengths of $20\tau_t$, $10\tau_t$, and $5\tau_t$, respectively. The three short time series have been specifically chosen because they feature a large fluctuation in the coarse grained quantity. Fig. 3d,e,f show the same in case of the zonal fields. The main finding is that up to moderately long averaging windows of about $10\tau_t$ (or $5\tau_x$ for spatial averages) it is possible to link large fluctuations with individual persistent events. When a coarser graining is considered, using a window of $20\tau_t$

for time averages and $10\tau_x$ or $20\tau_x$ for spatial ones, thus going in the direction of the regime of the large deviations discussed below, we do not have such an one-to-one identification. Instead, large ultralong fluctuations are related to the occurrence of subsequent moderately long persistent features.

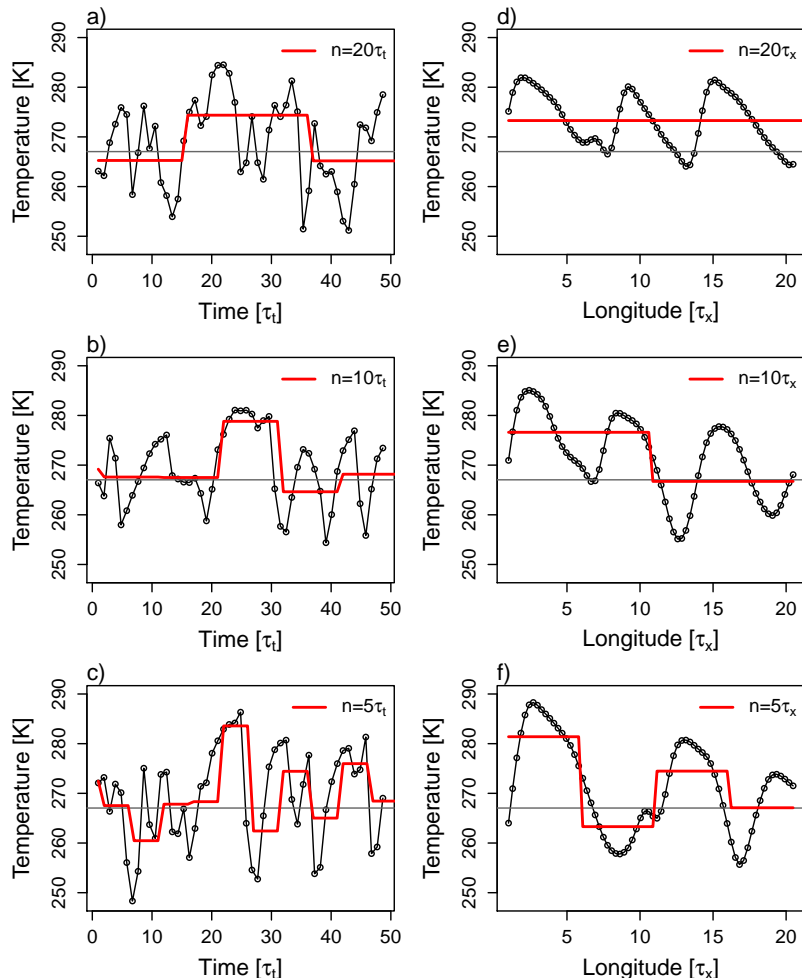


Figure 3: Relationship between persistent events and large fluctuations of the coarse-grained fields. a) Time series (black line) of near-surface temperature at 46° in the case of a large event of the coarse grained time series (red line) with averaging window of $20\tau_t$; x -axis in units of $\tau_t = 1.05$ days. b) Same as a), for averaging window of $10\tau_t$. c) Same as a), for averaging window of $5\tau_t$. d) Zonal series (black line) of surface temperature at 46° in the case of a large event of the coarse grained zonal series (red line) with averaging window of $20\tau_x$; x -axis in units of $\tau_x = 3.54$ grid points. e) Same as f), for averaging window of $10\tau_x$. f) Same as d), for averaging window of $5\tau_x$. In all panels the grey horizontal line represents the long term and longitudinal average.

4.1 The Link between Temporal and Zonal Large Deviations

At this point, we turn our attention to the estimation of the temporal and zonal rate functions. For this, we first have to obtain sequences of temporal and zonal averages for increasing lengths of averaging blocks n_t and n_x , for which we use the total length of our simulation of 10000 years.

$$A_{n_t} = \frac{1}{n_t} \sum_{i=1}^{n_t} T(x^*, y^*, t = i) \quad (16a)$$

$$A_{n_x} = \frac{1}{n_x} \sum_{i=1}^{n_x} T(x = i, y^*, t^*) \quad (16b)$$

The lengths of temporal averaging blocks are chosen to be multiples of τ_t : $n_t = 5\tau_t, 10\tau_t, \dots, 40\tau_t$. Similarly, the lengths of zonal averaging blocks are multiples of τ_x , but in this case the largest possible multiple m is limited due to the size and shape of the Earth, as mentioned above: $n_x = 5\tau_x, 10\tau_x, \dots, m\tau_x$. $m = 20$ in case of latitudes 60° and 46° , whereas $m = 10$ in case of latitude 30° . To increase the number of averaged values for the computation of the temporal rate functions, we lump together the temporal averages from every 25th longitude along a latitudinal circle. Since $\tau_x \ll 25$, these temporal sequences can be treated as independent repetitions. In case of zonal averaging, we take one averaged value in space from every 10th point along the time axis, which we consider to be independent repetitions as well. This assumption is a reasonable because the integrated temporal auto-correlation of zonal averages is much lower than 10, even for the largest n_x (as shown later in Fig. 5). We obtain for each value of n_t and n_x estimates of the rate functions, after using the re-normalising factors given by $1/\tau_t$ or $1/\tau_x$, respectively:

$$\tilde{I}_{n_t}(a) = -\frac{\ln p(A_{n_t} = a)}{n_t} \tau_t, \quad (17a)$$

$$\tilde{I}_{n_x}(a) = -\frac{\ln p(A_{n_x} = a)}{n_x} \tau_x, \quad (17b)$$

where $p(A_{n_t} = a)$ and $p(A_{n_x} = a)$ represent empirical estimates of the pdf's of the temporally and zonally averaged sequences. Due to the re-normalisation, the logarithm of the probabilities is scaled by n_t/τ_t or n_x/τ_x , i.e. by the number of uncorrelated instead by the total number of data in an averaging block. Thus, we eliminate the effect of correlations.

Figure 4 displays \tilde{I}_{n_t} (a–c) and \tilde{I}_{n_x} (d–f) for every n_t and n_x . As a side note, we remark that in every figure below the shown re-normalised rate function estimates are shifted vertically so that their minimum is at 0. In case of the temporal rate functions, it is clear that for $n_t \geq 20\tau_t$ the estimates \tilde{I}_{n_t} do not change in shape by further increase in n_t , meaning that we obtain stable and reliable estimates, i.e. there is a proof in our data for a LDP in time. We also notice that the range of A_{n_t} values becomes narrower as n_t increases as an effect of averaging, which reduces the amount of available data. Thus, we obtain our best estimate at an optimal averaging block length n_t^* which is large enough to allow for the convergence

of rate function estimates, but is in the same time small enough so that the range of A_{n_t} is not too narrow, i.e. $n_t^* = \min(n_t; \tilde{I}_{n_t} \approx I_{n_t})$. We choose the same optimal averaging length for all three latitudes $n_t^* = 20\tau_t$, although in case of latitudes 60° and 30° , $\tilde{I}_{n_t=10\tau_t}$ seems to be already a good estimate for the asymptotic I_{n_t} . In case of the zonal rate functions, we first notice that the largest n_x seems to be too small for a clear convergence. In other words, the length of a latitudinal circle is not long enough to clearly obtain a large deviation limit. However, the dependence of \tilde{I}_{n_x} on n_x seems to decrease as n_x is increasing, thus we choose the largest possible n_x as the optimal zonal averaging length $n_x^* = \max(n_x)$. $n_x^* = 20\tau_x$ in case of latitudes 60° and 46° , whereas in case of latitude 30° , n_x^* is only $10\tau_x$ because of stronger zonal auto-correlations.

The best estimates of the temporal and zonal re-normalised rate functions $\tilde{I}_{n_t}^* = \tilde{I}_{n_t=n_t^*}$ and $\tilde{I}_{n_x}^* = \tilde{I}_{n_x=n_x^*}$ are shown again in Fig. 4g,h,i. The shading represents the 95% confidence intervals of 2000 nonparametric ordinary bootstrap estimates based on the normal distribution (functions `boot` and `boot.ci` of the R package `boot`, Davison and Hinkley, 1997; Canty and Ripley, 2017). We notice that $\tilde{I}_{n_t}^* \approx \tilde{I}_{n_x}^*$. The equivalence is very good in case of latitude 60° and in case of negative anomalies at latitudes 46° and 30° . We also notice some differences in case of positive anomalies at latitudes 46° and 30° , with larger differences at 30° . At this later latitude, however, it has to be considered that the maximum possible zonal averaging length is $10\tau_x$, whereas in the other cases it is $20\tau_x$. We assume that the differences between the temporal and zonal re-normalised rate function estimates have to do with the fact that n_x^* is not large enough to estimate the rate function properly. Larger values of n_x are needed to overcome the enhanced skewness in the distribution of zonal averages as effect of spatial correlations, however this is impossible due to limitations coming from the size and shape of the Earth. These findings have correspondence with the large value of U_τ at this latitude, defining the anisotropy between space and time. While the temporal rate function can be estimated reliably at a relatively small n_t , the estimation of the zonal one is a much more difficult task.

However, the main message of Fig. 4 is that the temporal and zonal re-normalised rate functions seem to be equal, $I_{n_t} = I_{n_x}$, if the probability of averages is scaled by the number of uncorrelated data in an averaging block n_t/τ_t or n_x/τ_x , as explained above. In other words, there is a link connecting temporal and spatial large deviations or averages, due to the existence of a *universal function* I_n ; universal in the sense that it represents large deviations in both dimensions: time and space.

Obviously, based on the LDP in time or in space, one cannot characterise persistent temporal or spatial events, because the limit law starts to act on large scales, where persistence is lost and universality emerges. However, one can capture persistent space-time events by averaging in both dimension space and time. To achieve this, it is important that the spatial averaging length is not too small but not too large either, as we show in the following.

4.2 Spatio-temporal Large Deviations

We consider temporal sequences of zonally averaged observables over averaging lengths $n_x = 1\tau_x, 5\tau_x, 10\tau_x, 20\tau_x$, and then average each sequence in time for increasing averaging lengths $\hat{n}_t = 1\hat{\tau}_t, 5\hat{\tau}_t, 10\hat{\tau}_t, 15\hat{\tau}_t, \dots, 40\hat{\tau}_t$. The notation $\hat{\cdot}$ is meant to indicate that we average in space

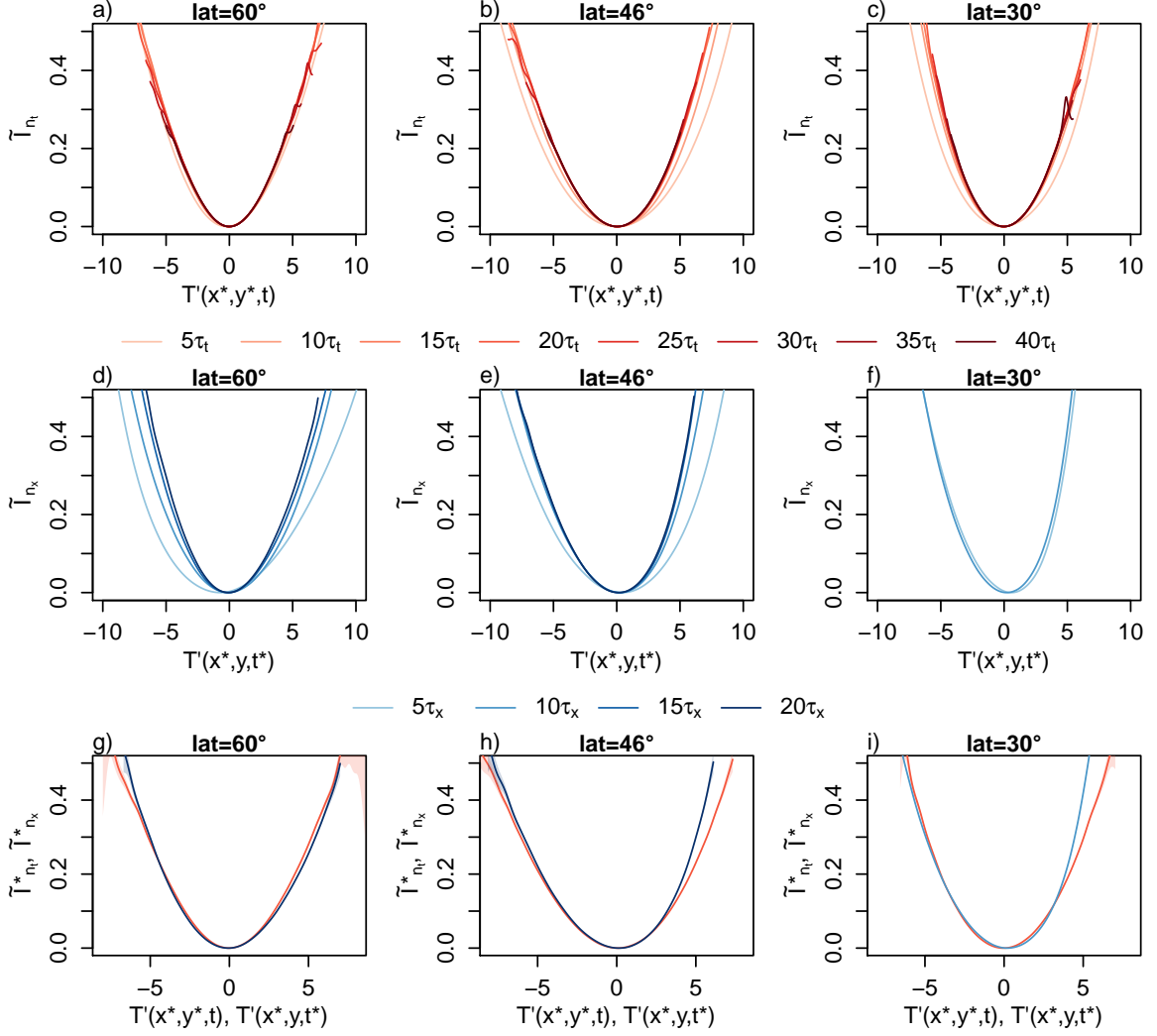


Figure 4: a) – c) Temporal re-normalised rate function estimates \tilde{I}_{n_t} and d) – f) zonal re-normalised rate function estimates \tilde{I}_{n_x} for the three considered latitudes and for increasing averaging lengths n_t and n_x according to the different colours (see legend). g) – i) Best estimates of the temporal (red) and zonal (blue) re-normalised rate functions. All estimates are shifted vertically so that their minimum is at 0.

and *additionally* in time and $\hat{\tau}_t$ is the decorrelation time of the spatially averaged observable. By considering several n_x values, we choose the spatial scale at which we analyse the large deviations in time. The spatio-temporal averages are computed as:

$$A_{n_x, \hat{n}_t} = \frac{1}{\hat{n}_t} \sum_{j=1}^{\hat{n}_t} \frac{1}{n_x} \sum_{i=1}^{n_x} T(i, y^*, j) = \frac{1}{\hat{n}_t} \sum_{j=1}^{\hat{n}_t} A_{n_x}(j). \quad (18)$$

Similarly to the previous cases, also in case of spatio-temporal averages, we have to take into account the strength of auto-correlations if we pursue to compare the spatio-temporal rate functions with the temporal and zonal ones. We estimate the integrated temporal auto-

correlation $\hat{\tau}_t$ of spatio-temporal averages analogously to τ_t or τ_x , but to assure the stability of $\hat{\tau}_t$ we choose a higher maximum lag of 120 days, because the auto-correlation in time of zonal averages has a slower decay compared to the one of unaveraged temporal or zonal observables. Fig. 5 shows $\hat{\tau}_t$ as function of zonal averaging length n_x and temporal averaging length \hat{n}_t . The temporal auto-correlations of the spatio-temporal observables are increasing with n_x and decreasing with \hat{n}_t . The increase with n_x , on the one hand, can be explained by the connection between temporal and spatial scales. Large events in space are long lasting events in time, as discussed in Sec. 1. The decrease of the temporal integrated auto-correlation with \hat{n}_t , on the other hand, can be explained by the increase of the number of uncorrelated events with respect to the number of correlated events in an averaging block as a consequence of increasing the block length. This is automatically the case for large averaging blocks when correlations are finite, and is crucial for the applicability of the block averaging method. The different behaviour with n_x and \hat{n}_t , however, has to do mainly with the discrepancies in the temporal resolution of the newly obtained averages. While, in case of zonal averaging, the temporal resolution remains one day, in case of additional averaging in time, the temporal resolution decreases with \hat{n}_t , thus the temporal auto-correlation lag increases. However, this is not a problem for our analysis since we are interested in the correlations of the averaged observables measured in number of averaged data. A stronger increase of $\hat{\tau}_t$ at the “end” of the channel underlines the above discussed effect of averaging along a latitudinal circle. At the zonal “end” of the channel the temperature values are strongly correlated with the ones at the “beginning” of the channel.

We observe the largest increase of $\hat{\tau}_t$ with n_x in case of latitude 60° . However, taking into account the different typical zonal scales at different latitudes and comparing the auto-correlations at same zonal averaging lengths in units of τ_x (for example along the vertical lines with same colours in Fig. 5) things look more similar. Here, we deliberately use the expression “more similar” instead of “the same” because the differences in the zonal tendencies are, of course, not only a matter of scale. The changing dynamical properties of the zonal mean temperature are determined by the latitudinal dependence of diabatic forcing, meridional heat transport due to eddy activity, zonal mean wind, static stability, etc.

Additionally, we also have to consider that the distance between the longitudes is decreasing from equator to pole due to the geometry of the sphere. This, of course, contributes to the fact that the temperature values at neighbouring longitudes are stronger correlated at latitude 60° than at 46° or 30° .

Estimates of spatio-temporal re-normalised rate functions are then computed for each n_x and \hat{n}_t as:

$$\tilde{I}_{n_x, \hat{n}_t}(a) = -\frac{\ln \tilde{p}(A_{n_x, \hat{n}_t} = a)}{\hat{n}_t n_x} \hat{\tau}_t \tau_x \quad (19)$$

We remark that Eq. (19) accounts for both zonal and temporal auto-correlations by multiplication with $\hat{\tau}_t \tau_x$, similarly to the case of temporal and zonal rate functions. The spatio-temporal re-normalised rate function estimates are displayed by Fig. 7 (coloured lines). For comparison reasons, we also show the best temporal and zonal estimates $\tilde{I}_{n_t}^*$ (continuous black lines) and $\tilde{I}_{n_x}^*$ (short-dashed black lines), together with the estimate of the zonal re-normalised rate function at the selected zonal averaging length \tilde{I}_{n_x} . The main message here

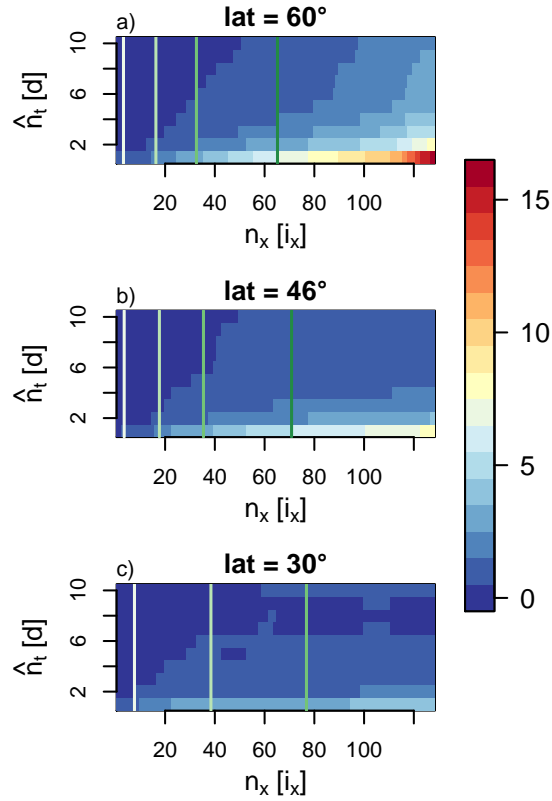


Figure 5: Integrated temporal auto-correlation of spatio-temporal averages for the selected latitudes as function of zonal and temporal averaging lengths. The vertical lines mark longitudes representing upper limits of zonal averaging (lower limit is 1), corresponding to the multiples of τ_x : $1\tau_x, 5\tau_x, 10\tau_x, 20\tau_x$ (from white to green).

is that:

- The spatio-temporal re-normalised rate function seems to be equal to the universal function I_n for *small* and *large* zonal averaging lengths.
- We suppose that in case of *small* zonal averaging lengths $n_x \ll n_x^*$, like $n_x = 1\tau_x$, the zonally averaged observable is not significantly different from the spatially localised observable, so that $\tilde{I}_{n_x, \hat{n}_t}$ converges to the universal function I_n .
- In case of *large* zonal averaging lengths $n_x \geq n_x^*$, like $n_x = 20\tau_x$, the zonal averages already exhibit universal characteristics, which are not altered by the additional temporal averaging, thus $\tilde{I}_{n_x, \hat{n}_t}$ corresponds again with the universal function I_n .
- On *intermediate* levels however, i.e. $\tau_x < n_x \leq n_x^*$, due to the non-trivial zonal correlations one obtains after zonal averaging a totally different observable from the original one.

The spatio-temporal re-normalised rate functions are different from the universal function I_n at $n_x = 5\tau_x$ in case of latitudes 60° and 46° , as well as $n_x = 10\tau_x$ in case of latitude 60° , whereas in this last case is worth mentioning that the spatio-temporal rate function corresponds with the zonal rate function estimate at $n_x = 10\tau_x$. In all these cases, the

spatio-temporal re-normalised rate functions are flatter than the universal function, pointing out a higher probability of large deviations, which are associated to the presence of organised structures. Thus, these scales are exactly the ones at which one can analyse persistent space-time events, like heat waves or cold spells, based on the LDP. Fig. 6 represents schematically the ranges of temporal and zonal averaging lengths, at which universality emerges (blue) or is hindered (light blue) due to zonal correlations. Pre-asymptotic regions, where the LDP is not valid yet, are left white.

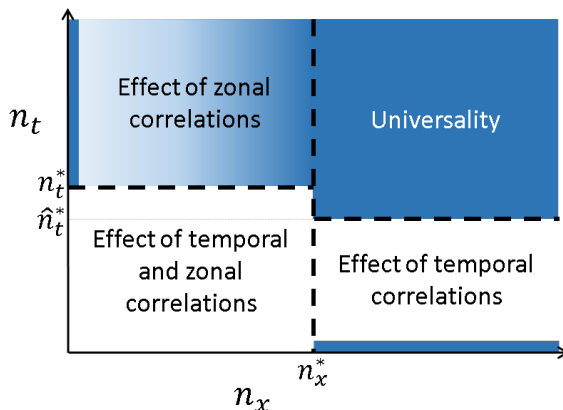


Figure 6: Schematic representation of universality and effect of correlations depending on the zonal and temporal averaging lengths. The dark blue colour marks the region where universality emerges. The light blue colour represents the region with non-universal spatio-temporal rate functions as an effect of zonal correlations. Pre-asymptotic regions, i.e. where the LDP is not valid yet, are white.

As a side note, the horizontal shift of the rate function estimates at small averaging lengths (n_x or \hat{n}_t) emphasise that these estimates are not reliable because the averaging length is too small for the law of large numbers to hold. We also wish to remark that differences emerge when looking at temperature data from latitude 30° . Here, the spatio-temporal re-normalised rate function $\tilde{I}_{n_x, \hat{n}_t}$ at $n_x = 1\tau_x$ is not equivalent with the universal function I_n . One possible reason for this is that when averaging over a length $n_x = 1\tau_x$ the newly defined observable has already significantly different properties from the temporal observable. The universality of the spatio-temporal rate function cannot be checked properly due to the limit in zonal averaging length of $10\tau_x$. What we see, however, is that at $n_x = 10\tau_x$ spatio-temporal re-normalised rate function is quite similar to - yet distinct from - the universal function.

4.3 Return Levels of the Large Deviations

We summarise shortly our main findings presented until now:

1. The estimates of the rate functions seem to converge to an asymptotic function, and we obtain the best estimate of the rate function at an optimal averaging block length n^* . This is mostly clear in case of the temporal rate functions, showing that there is a large deviation principle, i.e. a *universal law* that allows us to estimate the probabilities of occurrence of averages over $n \geq n^*$, without having to actually perform the averaging.

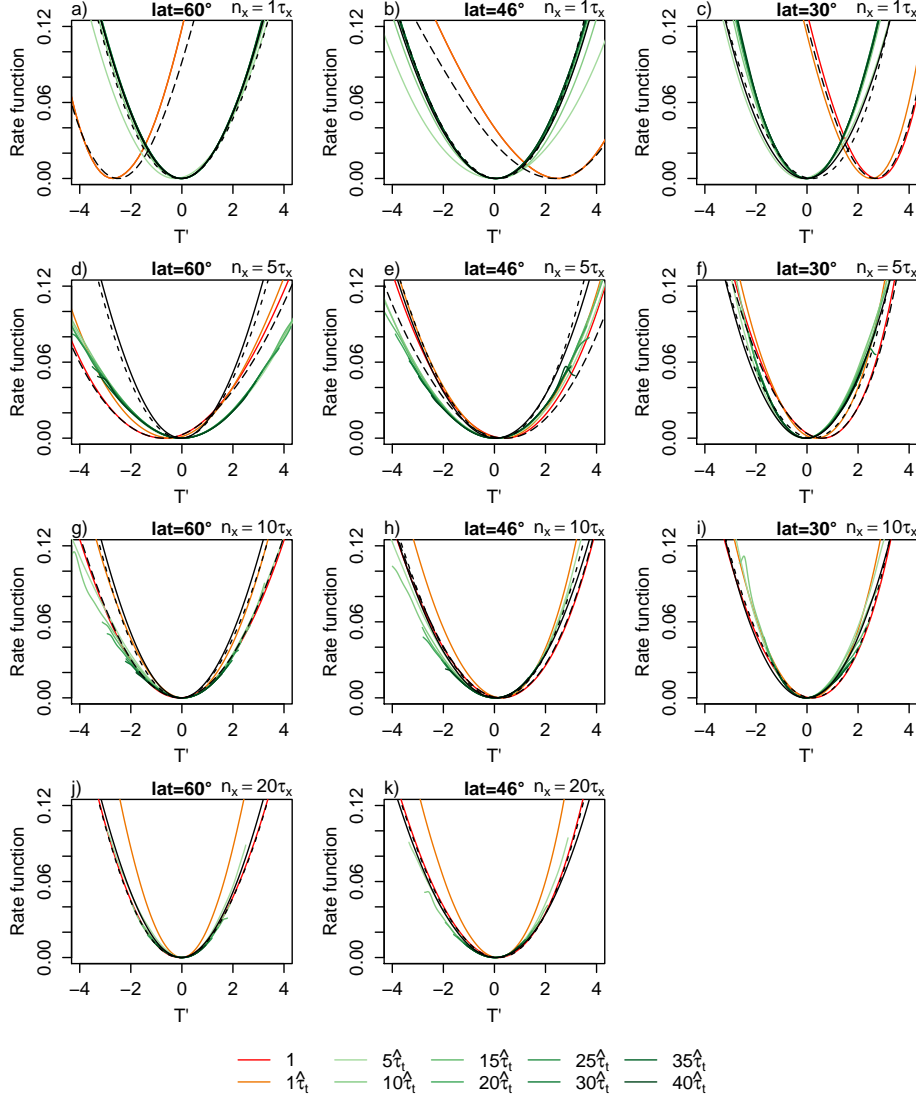


Figure 7: Rate functions of spatio-temporal averages for the selected latitudes and different zonal averaging lengths: a) – c) $n_x = 1\tau_x$, d) – f) $n_x = 5\tau_x$, g) – i) $n_x = 10\tau_x$, j) – k) $n_x = 20\tau_x$. The coloured lines represent spatio-temporal rate functions for different temporal averaging lengths \hat{n}_t according to the legend. The black continuous line is the best temporal rate function estimate, the black short-dashed line is the best zonal rate function estimate, and the black long-dashed line is the zonal rate function estimate at the selected n_x . The rate function estimates are shifted vertically so that their minimum is at 0.

2. We have found an *equivalence* between the temporal, spatial and spatio-temporal re-normalised rate functions, in the later case for very small and very large zonal averaging lengths. This means that we can deduce statistical properties of temporal averages from the ones of spatial averages and vice-versa. We can do the same in case of spatio-temporal averages and temporal or spatial averages.

Now, the question is how can we use these information in a practical way? One possibility

of application, which we present in this subsection by the example of latitude 60° , arises in the context of computing return periods of large events. Fig. 8 shows return level plots, i.e. return levels as function of return periods obtained in three different ways, based on: empirical data (circle markers), large deviation principle (continuous lines), and the Generalized Pareto distribution (dashed lines). For the estimation of return periods based on the LDP, we first obtain kernel density estimates (function `density` of the R package `stats`, R Core Team, 2016) of the pdf's $p(A_n = a)$ at fixed equidistant return levels $A_{n,1}, \dots, A_{n,256}$, based on which we estimate the cumulative distribution function $P(A_n \leq a)$, and then compute the return periods for $A_n \geq a$ as $\frac{1}{1-P(A_n \leq a)}$ and for $A_n \leq a$ as $\frac{1}{P(A_n \leq a)}$. Thus we obtain the return periods of both positive (Fig. 8a,c,e) and negative (Fig. 8b,d,f) large deviations. The shading around the continuous lines in Fig. 8 represents the 95% confidence intervals of 2000 nonparametric ordinary bootstrap return period estimates based on the normal distribution.

We compute the GPD return levels based on (5) using the maximum likelihood estimates of GPD parameters (functions `gpd.fit` and `gpd.rl` of the R package `ismev` functions written by Janet E. Heffernan with R port and documentation provided by Alec G. Stephenson., 2016). We analyse return levels of high temperature values exceeding a threshold equal to the 99.9 % quantile of the averaged series, as well as return levels of low temperature values below the 0.1 % quantile. To verify the applicability of the GPD method, the stability of return levels was checked also for a higher (lower) quantile of 99.99 % (0.01 %). The return level estimates seem to be stable even if the threshold is increased (not shown). Note that, although the very slow convergence of the GPD shape parameter is well known in some cases, the stability of return level estimates still holds if the change in the shape parameter is relatively small as the threshold increases (Galfi et al., 2017). The shading around the dashed lines in Fig. 8 represents 95% maximum likelihood confidence intervals of return level estimates. As a side note, in case of GPD the estimation concerns the return levels while the return periods are fixed, whereas we proceed the other way around in case of the LDP. This is necessary because we estimate the rate function $I(a)$ at fixed equidistant values a .

In Fig. 8a,b the return levels of temporal averages are shown for three different averaging windows $20\tau_t, 30\tau_t, 40\tau_t$. Here we use point 1. from above, and obtain the return periods based on the LDP *for every averaging window* from $p(A_{n_t^* = 20\tau_t} = a)$. We notice a very good agreement with the empirical data and the GPD return levels not only for $20\tau_t$ but also in case of $30\tau_t$ and $40\tau_t$, for both high (Fig. 8a) and low (Fig. 8b) extremes of averages. In case of $n_t = 20\tau_t$, the confidence intervals of the largest return periods based on the LDP become very unstable, the lower limits reach even negative values, thus they cannot be displayed on this semi-logarithmic scale.

The return periods from the LDP have an upper (or lower) limit because the estimation relies on empirical pdf's. This is not the case for the GPD return periods since these can be extrapolated to even unobserved events. The LDP, however, is a limit law that gives us return periods for every averaging length $n > n^*$, whereas the GPD return periods have to be computed separately for every n . This becomes more and more difficult with increasing n due to the decreasing data amount as effect of averaging. With other words, Fig. 8 points out the different dimensions in which the two limit laws act, as mentioned already in Sec. 1. The predictability of GPD is directed towards larger and larger events, i.e. towards unobserved ones, whereas the predictability of LDT is directed towards larger and larger averaging lengths, i.e. towards observables that, by construction, reduce dramatically the amount of data available for statistical analysis.

Point 2. presented above is illustrated by Fig. 8c,d and Fig. 8e,f. In the first case, return periods of temporal averages are computed based on the LDP obtained for zonal averages ($n_x^* = 20\tau_x$), and, in the second case, return periods of spatio-temporal averages (with a spatial averaging length of $20\tau_x$) are obtained from the LDP for temporal averages ($n_t^* = 20\tau_t$). In both cases, but especially for the spatio-temporal averages, the agreement with the empirical data and the GPD return levels is good. The differences between the return levels based on the LDP and the empirical data (also GPD) are related to the discrepancies in the estimation of the temporal and zonal, as well as temporal and spatio-temporal re-normalised rate functions. For example, the underestimation of low extremes of temporal averages based on the zonal rate function has to do with higher re-normalised zonal rate function values compared to the temporal ones in their left tails (see Fig. 4g).

We remark that the possibility of *commuting* between averages of different dimensions (time and space) is due to the fact that by eliminating the effect of serial correlations the large deviations of these different dimensions follow a *universal function*. This universal function, however, is inadequate to describe persistent space-time events, like heat waves or cold spells, because it acts on large scales, where persistence becomes irrelevant. To characterise the *persistent space-time events*, one needs to compute the temporal rate function of zonal averages *on intermediate scales*.

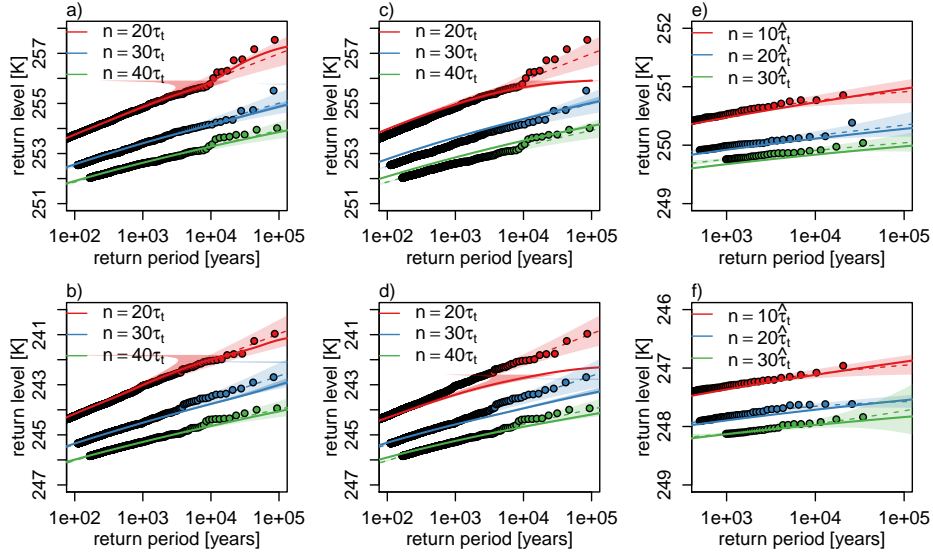


Figure 8: Return levels and return periods of a) – b) temporal and c) spatio-temporal large deviations of temperature at latitude 60° . Circle markers: empirical data; continuous line with shading: estimates based on LDT with 95% confidence intervals of 2000 nonparametric bootstrap samples based on the normal distribution; dashed line with shading: GPD estimates with 95% confidence intervals based on Maximum Likelihood Estimation. The different colours represent different averaging lengths. The LD-estimates are obtained based on a), c) temporal averages at $n_t^* = 20\tau_t$, and b) zonal averages at $n_x^* = 20\tau_x$.

5 Summary and Discussion

We have analysed the properties of temporal and spatial near-surface (960 hPa) temperature averages in the PUMA simplified global atmospheric circulation model based on LDT. Extremes of averages on specific scales are related to persistent extreme events, like heat waves or cold spells. We run the model for 10000 years with a constant (only latitude dependent) forcing, creating non-equilibrium (due to the forced-dissipative nature of the model) steady state simulations without orography, annual or daily cycle. The forcing is symmetric for the two hemispheres. The horizontal resolution is $T42$ with 10 vertical levels, and the temperature values are recorded daily. We compute and compare the re-normalised rate functions based on the integrated auto-correlation for temporal and zonal temperature sequences at selected latitudes (60° , 46° , and 30°), focusing in the mid-latitudes region, where turbulence is best developed. The spatial averaging is performed only in zonal direction, because this is geometrical direction along which the system has a symmetry. We also analyse the case of two-dimensional, i.e. spatio-temporal averaging. We verify the correctness of our results by comparing the return periods based on the rate functions with return periods from the empirical data and from the POT method. Before discussing them in detail, we summarise first our main findings:

1. The temperature averages in PUMA *follow a LDP*.
2. The temporal and zonal re-normalised rate functions are equal if we compute them by eliminating the effect of temporal and zonal correlations. Thus, we can define a *universal function*, describing temporal as well as spatial large deviations.
3. The spatio-temporal re-normalised rate functions are *equal* to the universal function for *small and large* spatial averaging lengths. *On intermediate levels*, as an effect of non-trivial spatial correlation, the spatio-temporal re-normalised rate functions *differ* from the universal one.

Our results show that the temperature averages in PUMA follow a LDP. The estimated rate functions clearly converge in case of temporal averages. We obtain reliable estimates at an optimal averaging length n_t^* , which is about $20\tau_t$, where τ_t represents the temporal integrated auto-correlation. The fact that the temperature averages follow a LDP might seem unsurprising, but actually it has extremely important consequences on a practical level. Based on the LDP, we can estimate the probabilities of averages, and thus for the practical use very important return periods, for every averaging length $n_t \geq n_t^*$. All we need to know is the probability of averages $A_{n_t^*}$, which we can estimate empirically. In contrast to the temporal averages, in case of zonal averaging the spatial averaging length n_x is substantially limited by the size and shape of a latitudinal circle. The temporal averaging is performed on a theoretically infinite (and practically very long) line, whereas the zonal averaging takes place on a circle. Thus, the convergence of the estimated rate functions is not that clear as for temporal averages. However, the comparison of the zonal results with the temporal re-normalised rate function estimates shows that the averaging length $n_x^* = 20\tau_x$ seems to provide a reasonable rate function estimate, thus we choose this one as the optimal zonal averaging length. In case of latitude 30° , $20\tau_x$ cannot be reached due to stronger zonal correlations. Here, the maximum averaging length is $10\tau_x$.

We find that the temporal and spatial re-normalised rate functions seem to be equal if we eliminate the effect of correlations according to Eq. (17), where we basically scale the rate

functions by the number of uncorrelated data instead of the whole number of data in an averaging block. Based on this equivalence, one finds a universal function $I_n = I_{n_t} = I_{n_x}$, in the sense that it describes both temporal and spatial large deviations. From a statistical-mechanical point of view, this means that fluctuations (around the steady state) in time and in space exhibit same basic properties, but differ as an effect of temporal and spatial persistence. From a practical point of view, this implies that one can commute between space and time: we can deduce statistical properties of spatial averages (including return level estimates) from a single time series, and this is, of course, true the other way round too.

Obviously, based on the LDP in one dimension - time or space - we cannot describe persistent events, because the limit law is acting on very large scales, where spatial or temporal organisation is lost and universality emerges. However, persistent space-temporal events can be studied based on LDT if one performs the averaging in both dimension - time and space.

Therefore, we extend our analysis also to spatio-temporal large deviations. Here, we average first in zonal direction taking different averaging lengths $n_x = 1\tau_x, 5\tau_x, 10\tau_x, 20\tau_x$, and then we search for a LDP in time of the zonally averaged observables. We find that the spatio-temporal re-normalised rate function, computed again by eliminating the correlations according to (19), is equal to the universal function I_n in two cases: 1) for small zonal averaging lengths $n_x \approx \tau_x$, and 2) for large ones $n_x \geq n_x^*$. We suppose that in the first case, due to the small n_x , the zonally averaged observable is not significantly different from the temporal observable, and thus the rate function converges to the universal function. In the second case, the zonal averages already exhibit universal characteristics because the large n_x allows for enough mixing in the series of zonal averages. These universal characteristics are not altered by the additional temporal averaging. On intermediate scales however, i.e. $\tau_x < n_x \leq n_x^*$, due to the non-trivial zonal correlations, one obtains after zonal averaging a totally different observable, whose large deviations follow a different rate function than the universal one. Consequently, by computing large deviations in time of zonal averages, we get rid of temporal persistence if the temporal averaging length is large enough, but we cannot eliminate the effect of zonal persistence on intermediate scales, which then leads to a non-universal re-normalised rate function. This also means that in this way we can study persistent extreme events based on LDT. These intermediate scales of about $5-10 \tau_x$ or $\approx 2000-4000$ km are approximately equal with the scale of persistent synoptic disturbances, like the ones causing severe heat waves. According to this points of view, long lasting synoptic scale disturbances are large deviations from the steady state, which allow for a higher degree of spatio-temporal organisation and, in a loose sense, a lower entropy compared to disturbances at any other scales.

Additionally, we compare the two frameworks for investigating rare events, i.e. LDT and the POT approach of EVT, from a practical point of view, based on return level and return period estimates. Both methods are based on limit laws, but they differ in the way the limit is obtained, and thus also in the direction in which the limit acts. The POT approach deals with the conditional probabilities of averages exceeding a high threshold. The limit law is obtained as one considers larger and large extremes, thus it is directed towards large, even unobserved events. In case of LDT, we approach the limit as we consider averages with increasing averaging length n , thus the limit is directed towards $n \rightarrow \infty$. Our results point out these differences. On the one hand, the return level estimates based on LDT are limited from above at small averaging lengths because they are obtained based on empirical distributions, whereas the estimates based on the POT approach can be extrapolated to unobserved events. On the other hand, the return levels based on LDT can be obtained for every $n \geq n^*$ based

on the probabilities of A_n^* , whereas in case of the POT approach they have to be estimated for every n separately. We also have to remark that the convergence to the limit law seems to be easier to achieve in case of LDT than in case of EVT (Galfi et al., 2017).

As mentioned above, we eliminate the effect of correlations in the computation of the rate functions by multiplication with the integrated auto-correlation. We estimate both temporal and zonal integrated auto-correlations, τ_t and τ_x . By computing the ratio between spatial and temporal persistence, we define a scale velocity $U_\tau = \tau_x/\tau_t$, which is a measure for the anisotropy between space and time. If the anisotropy between space and time is strong, it becomes more difficult to show the existence of a universal rate function. In case of latitude 30° , for example, due to a strong zonal persistence, the largest zonal averaging length is limited to $10\tau_x$, which is not large enough to obtain reliable estimates of the spatial rate function. We remark that the scale velocity we find by such asymptotic procedure could be viewed in connection with the research lines aiming at identifying the multifractal nature of the weather and climate fields (Lovejoy and Schertzer, 2013), and, in particular, of precipitative fields (Deidda, 2000).

While nature and society do not typically conform to the hypotheses of the theorems one needs to establish universal laws, such asymptotic results can nonetheless be extremely useful for studying observational data, just as in the widely studied case of EVT. Therefore, this work should be seen as a first step towards the use of large deviation theory for the analysis of actual climatic data and the outputs of state-of-the art climate models. The perspective is to find new ways to estimate efficiently the probability of occurrence of extremely rare events associated to persistent climatic conditions. In this work, we have focused on time scales which are long compared to those typical of the atmosphere, but one can adopt the same methods for studying persistent events of multiannual scales, where the oceanic variability is, instead, essential. This has, potentially, great relevance for addressing the problem of assessing human and environmental resilience to the low-frequency variability of the climate system.

Acknowledgements

The authors wish to thank T. Bódai for intellectual exchanges on the properties of extremes in geophysical flows, and F. Bouchet for stimulating conversations on the use of LDT for the study of geophysical flows. We would like to thank also E. Kirk and F. Lunkeit for providing help with the model simulations. VL acknowledges the support of the Sfb/Transregio project TRR181 "Energy Transfer in the Atmosphere and Ocean" and of the Horizon 2020 project "Blue Action". VMG acknowledges funding from the International Max Planck Research School on Earth System Modelling (IMPRS-ESM).

References

- Balkema, A. A. and L. de Haan, 1974: Residual life time at great age. *The Annals of Probability*, **2**, 792–804.
- Barriopedro, D., E. Fischer, J. Luterbacher, R. Trigo, and R. Garcia-Herrera, 2011: The hot summer of 2010: Redrawing the temperature record map of europe. *Science*, **332**, 220–224.
- Billingsley, P., 1995: *Probability and Measure*. Wiley, 3 edition.
- Bódai, T., 2017: *Extreme Value Analysis in Dynamical Systems: Two Case Studies*, Cambridge University Press. 392–429.
- Bouchet, F., C. Nardini, and T. Tangarife, 2014: Stochastic averaging, large deviations and random transitions for the dynamics of 2d and geostrophic turbulent vortices. *Fluid Dynamics Research*, **46**, 061416.
- Bouchet, F. and A. Venaille, 2012: Statistical mechanics of two-dimensional and geophysical flows. *Phys. Reports*, **515**, 227–295.
- Canty, A. and B. D. Ripley, 2017: *boot: Bootstrap R (S-Plus) Functions*. R package version 1.3-20.
- Castillo, E., 1988: *Extreme value theory in engineering*. Academic Press, New York.
- Coles, S., 2001: *An Introduction to Statistical Modeling of Extreme Values*. Springer Verlag.
- Cramer, H., 1938: Sur un nouveau théorème limite dans la théorie des probabilités. *Colloque consacré à la théorie des probabilités*, Hermann, Paris, volume 3, 2–23.
- Davison, A. C. and D. V. Hinkley, 1997: *Bootstrap Methods and Their Applications*. Cambridge University Press, Cambridge, iISBN 0-521-57391-2.
URL <http://statwww.epfl.ch/davison/BMA/>
- De Cruz, L., S. Schubert, J. Demaeyer, V. Lucarini, and S. Vannitsem, 2018: Exploring the lyapunov instability properties of high-dimensional atmospheric and climate models. *Nonlin. Processes Geophys.*, **2018**, 387412.
- Deidda, R., 2000: Rainfall downscaling in a space-time multifractal framework. *Water Resources Research*, **36**, 1779–1794.
- Dell’Aquila, A., V. Lucarini, P. M. Ruti, and S. Calmanti, 2005: Hayashi spectra of the northern hemisphere mid-latitude atmospheric variability in the ncep–ncar and ecmwf re-analyses. *Climate Dynamics*, **25**, 639–652, doi:10.1007/s00382-005-0048-x.
URL <https://doi.org/10.1007/s00382-005-0048-x>
- den Hollander, F., 2000: *Large Deviations*. American Mathematical Society.
- Donsker, M. and S. Varadhan, 1975a: Asymptotic evaluation of certain markov process expectations for large time. i. *Comm. Pure Appl. Math.*, **28**, 1–47.
- 1975b: Asymptotic evaluation of certain markov process expectations for large time. ii. *Comm. Pure Appl. Math.*, **28**, 279–301.
- 1976: Asymptotic evaluation of certain markov process expectations for large time. iii. *Comm. Pure Appl. Math.*, **29**, 389–461.

-
- 1983: Asymptotic evaluation of certain markov process expectations for large time. iv. *Comm. Pure Appl. Math.*, **36**, 183–212.
- Easterling, D., G. Meehl, C. Parmesan, S. Changnon, T. Karl, and L. Mearns, 2000: Climate extremes: Observations, modeling, and impacts. *Science*, **289**, 2068–2074.
- Eckmann, J. P. and D. Ruelle, 1985: Ergodic theory of chaos and strange attractors. *Rev. Mod. Phys.*, **57**, 617–656, doi:10.1103/RevModPhys.57.617.
URL <https://link.aps.org/doi/10.1103/RevModPhys.57.617>
- Ellis, R., 1984: Large deviations for a general class of random vectors. *Ann. Probab.*, **12**, 1–12.
- Embrechts, P., C. Klueppelberg, and T. Mikosch, 1997: *Modelling extremal events for insurance and finance*. Springer Verlag, Berlin.
- Fang, J.-Q. and G. Liu, 1992: Relationship between climatic change and the nomadic southward migrations in eastern asia during historical times. *Climatic Change*, **22**, 151–168, doi:10.1007/BF00142964.
URL <https://doi.org/10.1007/BF00142964>
- Faranda, D., G. Messori, and P. Yiou, 2017: Dynamical proxies of North Atlantic predictability and extremes. *Scientific Reports*, **7**, 41278.
- Ferro, C. A. T. and J. Segers, 2003: Inference for clusters of extreme values. *J. R. Statist. Soc. B*, **65**, 545–556.
- Fisher, R. A. and L. H. C. Tippett, 1928: Limiting forms of the frequency distribution of the largest or smallest member of a sample. *Proceedings of the Cambridge Philosophical Society*, **24**, 180–190.
- Fraedrich, K. and H. Boettger, 1978: A wavenumber-frequency analysis of the 500 mb geopotential at 50n. *Journal of the Atmospheric Sciences*, **35**, 745–750, doi:10.1175/1520-0469(1978)035<0745:AWFAOT>2.0.CO;2.
URL [https://doi.org/10.1175/1520-0469\(1978\)035<0745:AWFAOT>2.0.CO;2](https://doi.org/10.1175/1520-0469(1978)035<0745:AWFAOT>2.0.CO;2)
- Fraedrich, K., H. Jansen, E. Kirk, U. Luksch, and F. Lunkeit, 2005a: The planet simulator: Towards a user friendly model. *Meteorologische Zeitschrift*, **44**, 299–304.
- Fraedrich, K., E. Kirk, U. Luksch, and F. Lunkeit, 2005b: The portable university model of the atmosphere (puma): Storm track dynamics and low-frequency variability. *Meteorologische Zeitschrift*, **14**, 735–745.
- Fraedrich, K., E. Kirk, and F. Lunkeit, 2009: Puma portable university model of the atmosphere. Technical report, World Data Center for Climate (WDCC) at DKRZ.
URL https://doi.org/10.2312/WDCC/DKRZ_Report_No16
- functions written by Janet E. Heffernan with R port, O. S. and R. documentation provided by Alec G. Stephenson., 2016: *ismev: An Introduction to Statistical Modeling of Extreme Values*. R package version 1.41.
URL <https://CRAN.R-project.org/package=ismev>
- Galfi, V., T. Bódai, and V. Lucarini, 2017: Convergence of extreme value statistics in a two-layer quasi-geostrophic atmospheric model. *Complexity*, **2017**, 5340858.

-
- Gallavotti, G. and E. Cohen, 1995: Dynamical ensembles in stationary states. *Journal of Statistical Physics*, **80**, 931–970.
- Gärtner, J., 1977: On large deviations from the invariant measure. *Theory Probab. Appl.*, **22**, 24–39.
- Ghil, M. and W. Roberston, 2002: Waves vs. particles in the atmospheres phase space: A pathway to long-range forecasting? *PNAS*, **99**, 2493–2500.
- Giardina, C., J. Kurchan, V. Lecomte, and J. Tailleur, 2016: Simulating rare events in dynamical processes. *J. Stat. Phys.*, **145**, 787–811.
- Gnedenko, B., 1943: Sur la distribution limite du terme maximum d’une serie aleatoire. *Annals of Mathematics*, **44**, 423–453.
- Grieger, B., J. Segschneider, H. Keller, A. Rodin, F. Lunkeit, E. Kirk, and K. Fraedrich, 2004: Simulating titan’s tropospheric circulation with the portable university model of the atmosphere. *Advances in Space Research*, **34**, 1650–1654.
- Hayashi, Y., 1971: A generalized method of resolving disturbances into progressive and retrogressive waves by space fourier and time cross-spectral analyses. *Journal of the Meteorological Society of Japan. Ser. II*, **49**, 125–128, doi:10.2151/jmsj1965.49.2-125.
- Held, I. and M. Suarez, 1994: A proposal for the intercomparison of the dynamical cores of atmospheric general circulation models. *Bull. Amer. Meteor. Soc.*, **75**, 1825–1830.
- Herbert, C., 2015: An introduction to large deviations and equilibrium statistical mechanics for turbulent flows. *Stochastic Equations for Complex Systems: Theoretical and Computational Topics*, S. Heinz and H. Bessaih, eds., Springer, Switzerland.
- Holton, J. R., 2004: *An introduction to dynamic meteorology*. Elsevier Academic Press.
- Hosking, R. M., 1990: L-moments: Analysis and estimation of distributions using linear combination of order statistics. *J. R. Statist. Soc. B*, **52**, 105–124.
- Hoskins, B. and A. Simons, 1975: A multi-layer spectral model and the semi-implicit method. *Q. J. R. Meteorol. Soc.*, **101**, 637–655.
- Hvistendahl, M., 2012: Roots of empire. *Science*, **337**, 1596–1599, doi:10.1126/science.337.6102.1596.
URL <http://science.sciencemag.org/content/337/6102/1596>
- IPCC, 2012: *Managing the Risks of Extreme Events and Disasters to Advance Climate Change Adaptation*. Cambridge University Presse, [Field, C.B., V. Barros, T.F. Stocker, D. Qin, D.J. Dokken, K.L. Ebi, M.D. Mastrandrea, K.J. Mach, G.-K. Plattner, S.K. Allen, M. Tignor, and P.M. Midgley (eds.)]. A Special Report of Working Groups I and II of the Intergovernmental Panel on Climate Change.
- Katz, R. W., M. B. Parlange, and P. Naveau, 2002: Statistics of extremes in hydrology. *Advances in Water Resources*, **25**, 1287–1304, 25(8-12): 1287-1304.
- Kennett, D. J., S. F. M. Breitenbach, V. V. Aquino, Y. Asmerom, J. Awe, J. U. Baldini, P. Bartlein, B. J. Culleton, C. Ebert, C. Jazwa, M. J. Macri, N. Marwan, V. Polyak, K. M. Prufer, H. E. Ridley, H. Sodemann, B. Winterhalder, and G. H. Haug, 2012: Development and disintegration of maya political systems in response to climate change. *Science*, **338**,

788–791, doi:10.1126/science.1226299.

URL <http://science.sciencemag.org/content/338/6108/788>

- Klein, R., 2010: Scale-dependent models for atmospheric flows. *Annu. Rev. Fluid Mech.*, **42**, 249274.
- Leadbetter, M. R., I. Weissman, L. de Haan, and H. Rootzen, 1989: On clustering of high values in statistically stationary series. *Proceedings of the 4th International Meeting on Statistical Climatology*, J. Sansom, ed., New Zealand Meteorological Service, Wellington, 217–222.
- Lestang, T., F. Ragone, C. Brehier, C. Herbert, and F. Bouchet, 2018: Computing return times or return periods with rare event algorithms. *J. Stat. Mech.*, **2018**, 043213.
- Lovejoy, S. and D. Schertzer, 2013: *The weather and Climate: emergent laws and multifractal cascades*. Cambridge U. Press.
- Lucarini, V., R. Blender, C. Herbert, F. Ragone, S. Pascale, and J. Wouters, 2014: Mathematical and physical ideas for climate science. *Rev. Geophys.*, **52**, 809859.
- Lucarini, V., D. Faranda, A. C. M. Freitas, J. M. Freitas, M. Holland, T. Kuna, M. Nicol, M. Todd, and S. Vaienti, 2016: *Extremes and Recurrence in Dynamical Systems*. Wiley.
- Lucarini, V., K. Fraedrich, and F. Lunkeit, 2010: Thermodynamic analysis of snowball earth hysteresis experiment: Efficiency, entropy production and irreversibility. *Quarterly Journal of the Royal Meteorological Society*, **136**, 2–11, doi:10.1002/qj.543.
- Lunkeit, F., K. Fraedrich, and S. Bauer, 1998: Storm tracks in a warmer climate: sensitivity studies with a simplified global circulation model. *Clim. Dynamics*, **14**, 813–826.
- Messori, G., D. Faranda, and R. Caballero, 2017: A dynamical systems approach to studying midlatitude weather extremes. *Geophys. Res. Lett.*, **44**, 3346–3354.
- Mikosch, T. and A. Nagaev, 1998: Large deviations of heavy-tailed sums with applications in insurance. *Extremes 1*, **1**, 81–110.
- Oono, Y., 1989: Large deviation and statistical physics. *Progr. Theoret. Phys. Suppl.*, **99**, 165–205.
- Pickands, J., 1975: Statistical inference using extreme order statistics. *The Annals of Statistics*, **3**, 119–131.
- Poumadere, M., M. Claire, S. Le Mer, and R. Blong, 2005: The 2003 heat wave in france: Dangerous climate change here and now. *Risk Analysis*, **25**, 1483–1494, doi:10.1111/j.1539-6924.2005.00694.x.
URL <https://onlinelibrary.wiley.com/doi/abs/10.1111/j.1539-6924.2005.00694.x>
- R Core Team, 2016: *R: A Language and Environment for Statistical Computing*. R Foundation for Statistical Computing, Vienna, Austria.
URL <https://www.R-project.org/>
- Ragone, F., J. Wouters, and F. Bouchet, 2017: Computation of extreme heat waves in climate models using a large deviation algorithm. *PNAS*, **115**, 24–29.

-
- Robinson, P., 2001: On the definition of a heat wave. *J. Appl. Met.*, **40**, 762–775.
- Rohwer, C., F. Angeletti, and H. Touchette, 2015: Convergence of large-deviation estimators. *Phys. Rev. E*, **92**, 052104.
- Segers, J., 2005: Approximate distributions of clusters of extremes. *Stat. and Prob. Letters*, **74**, 330–336.
- Sillmann, J., M. Croci-Maspolli, M. Kallache, and R. Katz, 2011: Extreme cold winter temperatures in europe under the influence of north atlantic atmospheric blocking. *J. Climate*, **24**, 5899–5913.
- Speranza, A., 1983: Deterministic and statistical properties of the westerlies. *pure and applied geophysics*, **121**, 511–562, doi:10.1007/BF02590154.
URL <https://doi.org/10.1007/BF02590154>
- Stefanon, M., F. D’Andrea, and P. Drobinski, 2012: Heatwave classification over europe and the mediterranean region. *Environ. Res. Lett.*, **7**, 014023.
- Touchette, H., 2009: The large deviation approach to statistical mechanics. *Physics Reports*, **478**, 1–69.
- Vannitsem, S. and V. Lucarini, 2016: Statistical and dynamical properties of covariant lyapunov vectors in a coupled atmosphereocean model multiscale effects, geometric degeneracy, and error dynamics. *J. Phys. A-Math. Theor.*, **49**, 224001.
- Vautard, R., P. Yiou, F. D’Andrea, N. de Noblet, N. Viovy, C. Cassou, J. Polcher, P. Ciais, M. Kageyama, and Y. Fan, 2011: Summertime european heat and drought waves induced by wintertime mediterranean rainfall deficit. *Geophys. Res. Lett.*, **34**, L07711.
- WHO, 2004: Heat-waves: risks and responses. *Health and Global Environmental Change*, **2**.
- Wouters, J. and F. Bouchet, 2016: Rare event computation in deterministic chaotic systems using genealogical particle analysis. *J. Phys. A: Math. Theor.*, **49**, 374002.
- Zahid, M., R. Blender, V. Lucarini, and M. C. Bramati, 2017: Return levels of temperature extremes in Southern Pakistan. *Earth Syst. Dynam. Discuss.*, **8**, 1263–1278.